Air-Conditioning, Heating and Refrigeration Technology Institute

Final Report

AHRTI Report No. 20110-01

VOID FRACTION AND PRESSURE DROP MEASUREMENTS FOR REFRIGERANT R410A FLOWS IN SMALL DIAMETER TUBES

Final Report

Date Published – October 2012

Timothy A. Shedd

UNIVERSITY OF WISCONSIN - MADISON
Multiphase Visualization and Analysis Laboratory
1500 Engineering Drive
Madison, WI 53706-1609

Prepared for

AIR-CONDITIONING, HEATING AND REFRIGERATION TECHNOLOGY INSTITUTE, INC
2111 Wilson Boulevard, Suite 500, Arlington, Virginia 22201-3001

DISCLAIMER

This report was prepared as an account of work sponsored by the Air-Conditioning, Heating and Refrigeration Technology Institute, Inc. (AHRTI). Neither AHRTI, its research program financial supporters, or any agency thereof, nor any of their employees, contractors, subcontractors or employees thereof - makes any warranty, expressed or implied; assumes any legal liability or responsibility for the accuracy, completeness, any third party's use of, or the results of such use of any information, apparatus, product, or process disclosed in this report; or represents that its use would not infringe privately owned rights. Reference herein to any specific commercial product, process, or service by trade name, trademark, manufacturer, or otherwise, does not necessarily constitute nor imply its endorsement, recommendation, or favoring by AHRTI, its sponsors, or any agency thereof or their contractors or subcontractors. The views and opinions of authors expressed herein do not necessarily state or reflect those of AHRTI, its program sponsors, or any agency thereof.

Funding for this project was provided by (listed alphabetically):
- Air-Conditioning, Heating and Refrigeration Institute (AHRI)
- Copper Development Association (CDA)
- Heating, Refrigeration and Air Conditioning Institute of Canada (HRAI)
- New York State Energy Research and Development Authority (NYSERDA)

Executive Summary

The objective of this project was to measure the pressure drop and void fraction of R-410A at condensation conditions (i.e., $T_{sat} \sim 50$ °C) in small, single tubes of 0.5 mm, 1 mm and 3 mm in diameter. The project was to deliver models for these behaviors as well.

As is detailed in the following report, the PI and his staff achieved these objectives along with several other significant outcomes. These are summarized here:

- A ring-sensor capacitance probe was used for the first time at length scales of 3 mm and below, and a new, general method was developed for calibrating the probe in-situ, greatly increasing the accuracy and utility of the capacitive void fraction sensor
- A unique micro-channel flow facility was developed in which the flow of liquid and vapor are independently driven by separate high-pressure syringe pumps, allowing for very stable two-phase flow at a wide range of flow conditions and flow rates. In addition, this eliminated the very challenging problem of accurately measuring very small flow rates of vapor or liquid.
- As a result of the flow visualization, it was discovered that droplet entrainment is very significant in microchannel flows. The PI has not seen this behavior clearly documented in previous literature. Droplets sizes do not scale with tube diameter, so droplets with diameters that are 50% or more of the tube diameter are not uncommon in the 0.5 mm tube flows. This observation led to modeling efforts that were very successful in capturing the diameter trends in the pressure drop and void fraction.
- In order to be able to develop models with confidence, the PI and his staff extended the scope of the project to include data at $T_{sat} \sim 30$ °C. The reason for this is that the thermophysical properties of R-410A are very sensitive to temperature, and this allowed the investigators to probe the impact of these properties on the pressure drop and void fraction in addition to the impact of geometry and flow rate.
- This report presents a new interpretation of the Muller-Steinhagen and Heck correlation for pressure drop and a simple modification that allows it to accurately predict pressure drop and pressure drop trends (i.e., the peak in the pressure drop vs. quality curve) as the tube diameter decreases. While still heavily empirical, the result is general and should still retain its accuracy for large tube flows as well. This model predicted all of the current data set (no data excluded) to within 17% MAE as well as capturing all of the trends in the data correctly.
- The void fraction data indicated, in agreement with many previous researchers, that as the tube diameter decreases, the void fraction behavior

approaches that of a homogeneous mixture. However, at mid to high qualities, the void fraction reverts to "large tube" or separated flow behavior. The detailed data provided in this report are the first such data ever produced for small tubes and provide important insight into the void fraction behavior. A new model has been developed based on the data and the flow visualization that predicts the void fraction from all test sections and flows (no data excluded) to within 7% MAE. This model will extend to large tubes without modification. It is based on physical principals and appears to capture all tube geometry and fluid property variations extremely well.

Recommendations

Based on the extensive experience gained from this project, the PI recommends the following for future studies:

- Continue this work to smaller tubes and wider flow ranges using the new test facility design. This design is very flexible and can operate over a wider range of conditions than other designs reported in the literature.
- Fully characterize the entrainment behavior. It is hypothesized that droplet entrainment plays an increasingly dominant role in the two-phase flow behavior as the test section diameter decreases. Models are needed for droplet size and velocity over a wide range of operating conditions and fluid properties.
- Focus on development of a physical, phenomenological model for pressure drop in two-phase flow. It is likely that additional models for entrainment, wave generation and wave shear, among other items, will be needed.
- Explicitly incorporate entrainment into the void fraction model. With detailed droplet entrainment data, it is likely that an accurate, first-principles model can be developed for void fraction.
- It will be vitally important to add the effects of applied heat flux, both in evaporation and condensation, to this analysis. Heat flux will add significant acceleration and instability to the flow as well as impact droplet entrainment. In evaporation, the impact of a rapidly moving three-phase contact line must be quantified.

Table of Contents

1.0 Introduction

This project was motivated by the need to obtain reliable void fraction data for two-phase flows of R-410A in small channels ranging from 0.5 mm to 3 mm at conditions similar to those of an air-conditioning or refrigeration condenser. In addition, improved pressure drop models were sought for these geometries and flow conditions. It was stipulated that single channel data be obtained, which posed unique challenges in experimental design and data acquisition.

It should be noted from the outset that void fraction and pressure drop are only indirectly related. The void fraction can best be thought of as being an indicator of relative shear in a vapor-liquid flow. But one only need to consider that there is a very limited range of values that void fraction can take on to realize that there is not a unique relationship between void fraction and pressure loss. Instead, shear is established between the phases as the vapor accelerates past the liquid and this shear determines how thin the liquid becomes at the wall, what types of waves are formed, the concentration of droplets, etc., that all determine void fraction. Void fraction may be used as a component of a pressure drop model, but its usefulness will lie in indicating the type of shear model to impose rather than being an integral part of the calculation necessarily. For example, at low void fraction, it is likely that the flow regime is bubbly, and thus an interfacial area model is required along with models for the physics of bubble break-up and distribution. The void fraction can be used to close this model, but could also be derived from the components of the model independently. If annular flow is present, the void fraction is often used to estimate a film thickness which is then used to determine a shear. However, this approach is fundamentally inaccurate. The interfacial and wall shears are not well represented by a single mean value but rather by a distribution of values that are related to the dynamics of the interface and the entrainment of one phase into another (Shedd 2013). The value of the void fraction data and models in this study lie in the ability to predict how the refrigerant charge is distributed in an air-conditioning or refrigeration system.

This report describes first the experimental apparatuses that were fabricated to generate the void fraction and pressure drop data. Two different setups were used due to limitations in the ability to reach either extreme of flow with one type of setup. Next, the basic flow behaviors are discussed qualitatively to provide context for the detailed discussion of pressure drop that follows. The pressure drop data are compared to some established correlations, but it is found that a modified form of the correlation by Müller-Steinhagen and Heck (1986) works very well with the current data. This modification is based on a new interpretation of the physical behaviors that may underlie this successful correlation. The void fraction measurement is presented next, with a detailed presentation of the calibration of the ring-capacitance sensor implemented in this facility. A novel in-situ calibration was developed as no static calibration can adequately capture the dynamics of two-phase flow or the changing dielectric constants of the fluids. Finally, the void fraction data are presented and found to exhibit more subtle behavior than has been suggested in previous studies. A new model is developed that combines the behaviors of the homogeneous equilibrium model and the separated flow model (represented by Rouhani-Axelsson) with very successful prediction of the current data set.

2.0 Experimental Setup

2.1 2.92 mm I.D. Flow Facility

The schematic of the R-410A flow facility is shown in Figure 1. The refrigerant loop consists of two sections: the test and recirculation sections. The test section of the loop consists of one needle valve that helps to control the flow, a Coriolis mass flow meter (Micromotion Elite Sensor CMF 010) that measures with an accuracy of 1.35% and 0.1% of the rate for the smallest and biggest flow rate, respectively, a 1000 W cartridge heater (257.9 mm long × 18.8 mm diameter), and the condenser-receiver. The actual test section is made out of a stainless-steel tube of 2.92 mm I.D. and 0.2685 m in length. The heater was powered by a Xantrex 600-10 6000 W precision DC power supply.

A picture of the test section, viewing section, and void fraction section can be seen in Figure 2. The test section was designed to achieve the mass fluxes desired with the flow controller and the ball valve before the filter in the recirculation loop that helps to control the flow as well. The pressure gradient through the test section is measured by a differential pressure transmitter (Yokogawa EJA110A) which has an accuracy of ± 75 Pa. Pressure taps were constructed by drilling four 600 μm holes in the test section tube. This was done in order to account for the pressure distribution around the tube and the fact that the thermocouples would basically cover one of these holes. Two tees at the start and end of the test section were used to interface with the pressure sensors. Figure 2 shows this setup in the R410A loop and Figure 3 shows the test section for the 2.96 mm I.D. tube.

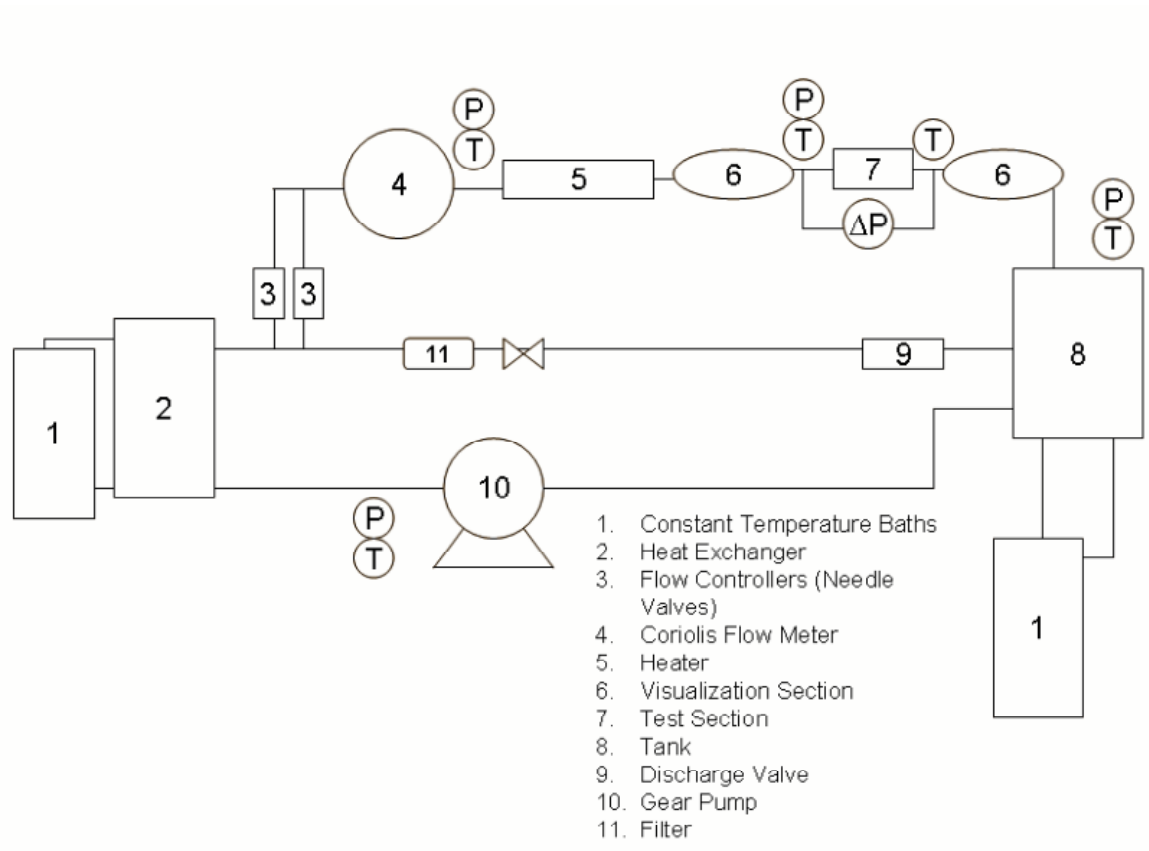

Figure 1: Schematic of flow facility for the 2.96 mm test section.

The recirculation section consists of a gear pump (Micropump GC M25) with a displacement of 1.89 ml/rev, a compact heat exchanger (Flat plate CH1/2A-XP) rated at 650 psi for R-410A, a filter, and a controlling valve before the filter. The purpose of this section of the facility is to circulate liquid between the pre-conditioning heat exchanger and the reservoir to keep the properties of the working fluid constant. By ensuring that the flow through the recirculation loop is much larger than that through the test section, pressure and temperature fluctuations that may occur due to the phase change are minimized. The saturation temperature and pressure are controlled by two Cole-Parmer Polystat constant temperature circulating water baths. One bath with a 1000 W capacity maintains the temperature of the refrigerant condenser-receiver after the test section. The other, with a capacity of 300 W, is used to pre-condition the refrigerant entering the test section. Controlling these two separately, the temperature of the refrigerant entering the test section can be maintained with a deviation of only 0.2 K from the desired test section temperature for quality ranging from 0 to 100%.

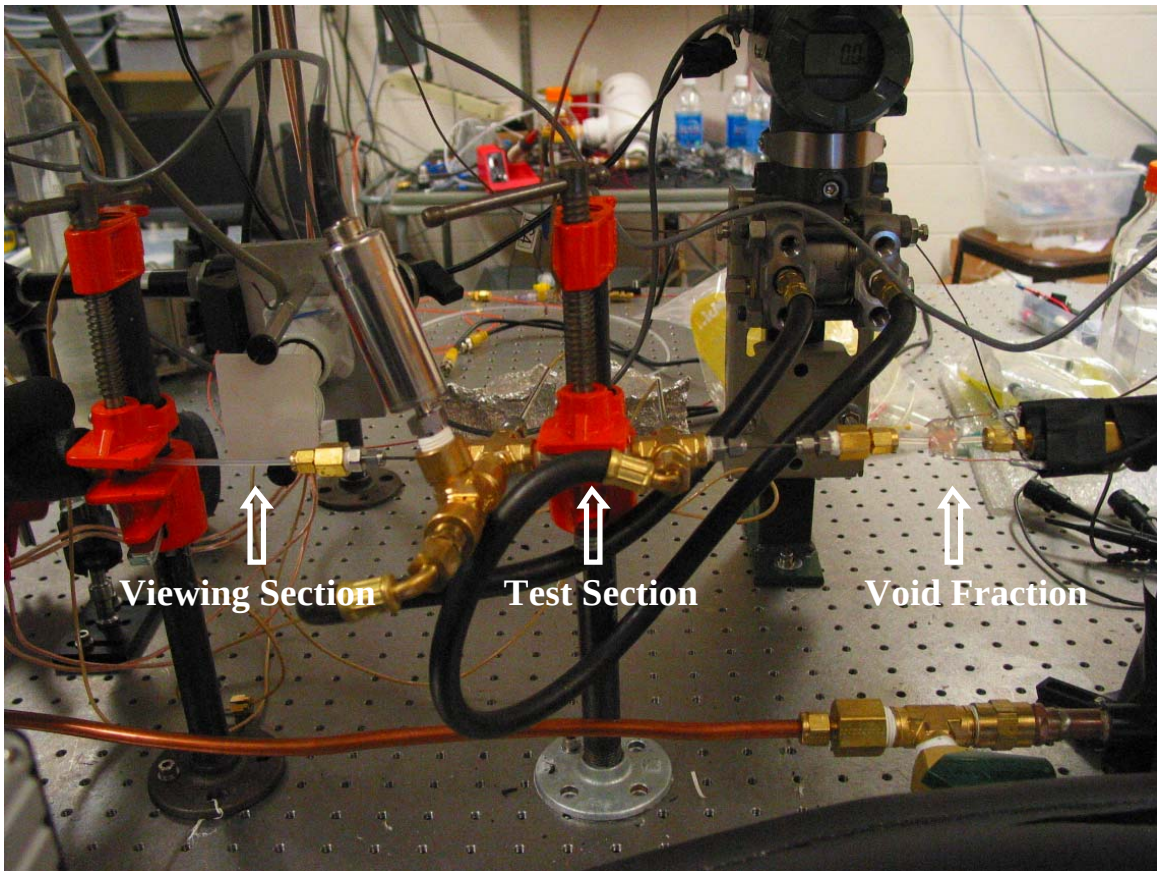

Figure 2: Photo of test section placement in the facility.

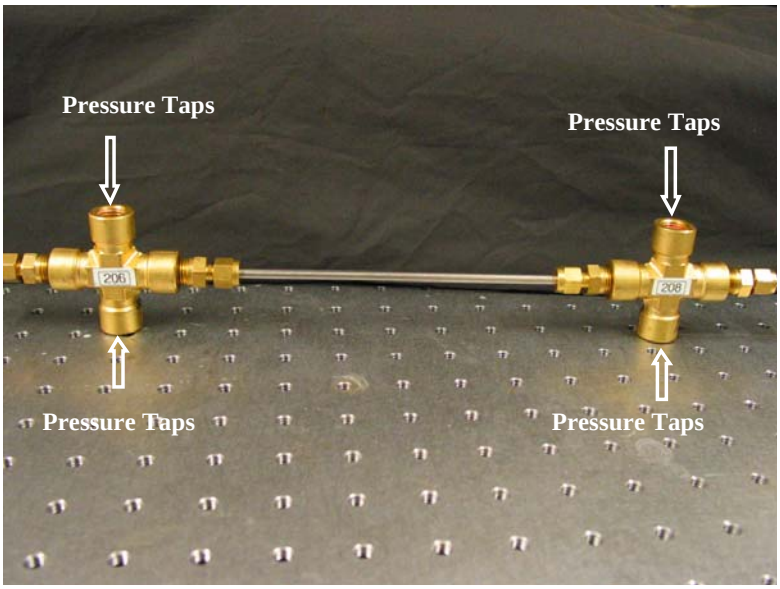

Figure 3: Photo of test section with pressure tap interface tees.

Absolute pressure measurements were performed with Cole-Parmer absolute pressure transducers, model 68072-58 with a range of 0 to 3.45 MPa absolute (0 to 500 psia) and an accuracy of +/- 8600 Pa. Thermocouples employed special limits of error wire and were calibrated using the precision temperature baths to within 0.2 °C mean absolute accuracy from 5 °C to 90 °C. The saturation temperature could be determined by the pressure measurement to within 0.2 °C for the 30 °C condition and 0.12 °C for the 50 °C condition. Thus, steady state was only assumed when the thermocouple at the entrance to the test section matched the pressure reading at the same location to within about 0.3 °C.

Precision in the measurements is achieved by keeping the conditions desired stable in the flow loop as it can be observed in Figure 4. This shows test section temperature stability at 30 °C and a mass flow rate of 2.8 g /s versus the number of data points for the 2.96 mm I.D. tube.

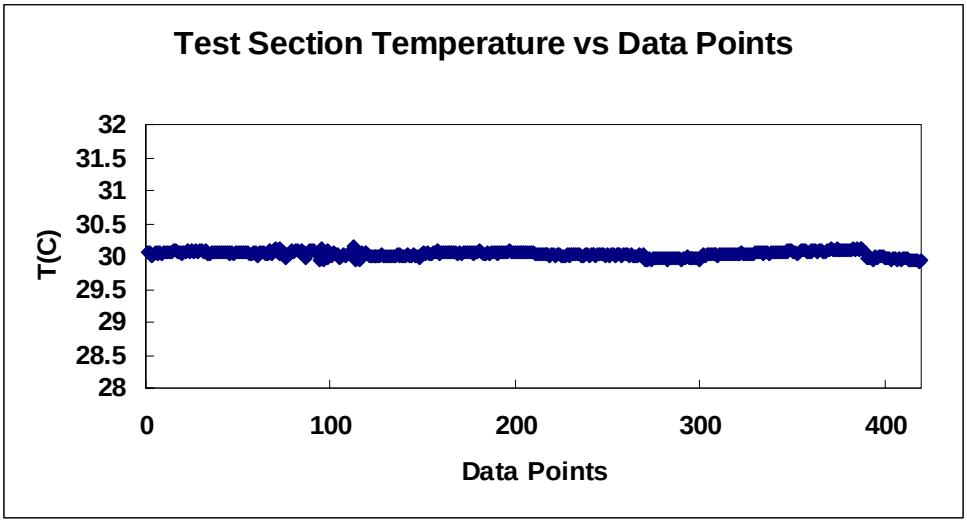

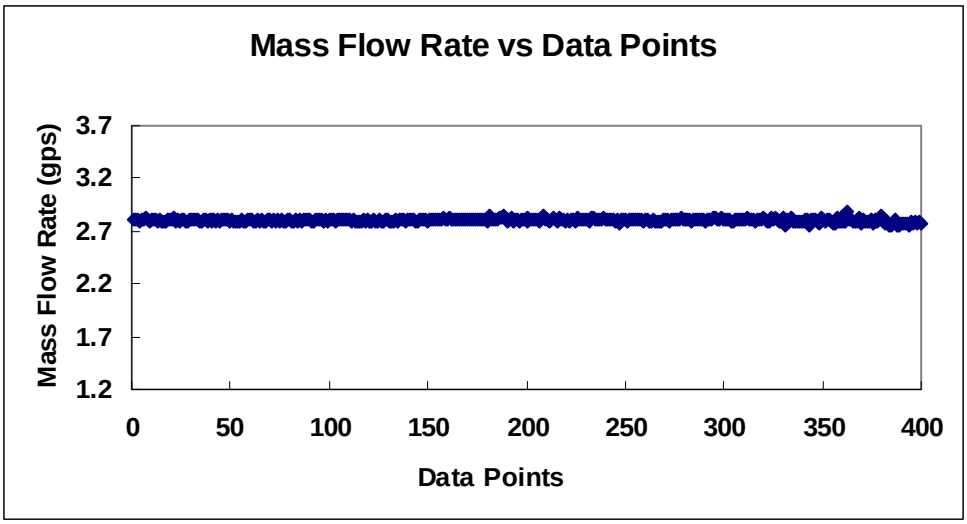

Figure 4: Stability of the 2.92 mm flow facility.

Except for the visualization section, the entire facility was insulated using closed cell urethane foam. In order to minimize heat losses from the test section, a 3/16" copper tube ran parallel to it within the insulation carrying water from a separate temperature controlled circulating bath at the desired operating temperature (30 °C or 50 °C). Temperature and pressure measurements obtained at the beginning of the pressure drop measurement were used to verify that the two-phase mixture was in saturation at the desired operating condition (as can be seen in Figure 4) within the uncertainty of the pressure and temperature transducers.

The experimental uncertainty for the pressure gradient is estimated to be ±8.5% based on both the bias error of the transducer and the standard deviation from the mean for all the data presented in this study. The uncertainty in the mass flow rate calculated similarly was ±1.5% for the 3 mm tube. An uncertainty propagation was performed to determine the impact of variations in saturation temperature, and subsequently fluid properties (i.e., μ, ρ), on the pressure gradient. It was found that, for every ±1°C in the saturation temperature, there is an approximate ±1.5% variation in viscosity, a ±3% variation in density and a ±2% variation in the pressure gradient. To see how the saturation temperature impacts the pressure gradient, it is assumed, as in many two-phase pressure drop correlations, that the pressure drop is essentially proportional to some two-phase friction factor (*f*) times the vapor kinetic energy $\rho_g V_g^2$, as shown in Equation (1).

$$\Delta P = \gamma f \rho_g V_g^2 \tag{1}$$

If this equation is rearranged further, it can be observed that pressure drop has a significant inverse proportionality to density and a weak direct proportionality to viscosity, making the pressure gradient very sensitive to the changes in density of the vapor. The changes in viscosity affect the change in pressure, but not significantly compared to the changes in density, as it can be observed in Equation (2) in the exponent of μ_l.

$$\Delta P = \gamma \frac{\mu_l^{0.25}}{\rho_g} G^{1.75} \quad (2)$$

In Equations (1) and (2), the term γ represents a constant of proportionality. A study of all the sets of empirical data was performed comparing the pressure gradient at the same qualities and mass flux, and it was found that the changes in density from saturation conditions at 30°C and 50°C account for 80% of the variations in the pressure drop. This observation provides a good understanding of what the important parameters are when studying pressure drop and how important it is to maintain the saturation temperature within minimal deviation.

It was also found by means of an uncertainty propagation analysis for the quality that, due to variations in temperature and mass flow rate, the uncertainty in the measured quality is ±2% and depends greatly on the variation of temperature, as the uncertainty in the mass flow rate is relatively small.

Uncertainty in void fraction was calculated by means of an uncertainty propagation of the measured values of capacitance that constitute the normalized capacitance, which is directly correlated to void fraction. The mean of all averaged standard deviations for each data point per void fraction data set was considered as the total uncertainty when calculating the propagation of uncertainty of the capacitance measurements to the void fraction. These calculations were done using the Engineering Equation Solver (EES) software. The results of these calculations for the different mass fluxes, temperatures, and both sizes of tubes studied in this work are shown in Table 1.

Table 1: Void Fraction Uncertainty

G	T	Uncertainty 3mm	Uncertainty 1mm
[kg m^{-2} s^{-1}]	[°C]	[± %]	[± %]
200	30	0.58	3.5
200	50	0.46	3.7
400	30	0.43	3.1
400	50	0.53	2.7
600	30	0.46	4.0
600	50	0.45	3.8
800	30	0.59	3.3
800	50	0.60	4.3

2.2 Single Phase Verification

In order to verify the accuracy and operation of the R-410A flow facility, a series of tests were done in single-phase liquid, which was accomplished by turning on the gear pump and letting the liquid reach steady state without providing any heat to the refrigerant. Single phase pressure drop measurements were taken for the 2.92 mm tube at 10, 30, and

35°C and flow rates were varied from 0.0022 kg s^{-1} to 0.022 kg s^{-1}. The results were then compared to single-phase pressure drop predictions using the Churchill (1977) friction factor with a tube roughness of 3 microns. The roughness value is within the range recommended by White (1999) for stainless steel tubing. Figure 5 shows the agreement between the experimental data and the correlation for the 2.92 mm tube. The error obtained from the comparison was less than 4% mean absolute error.

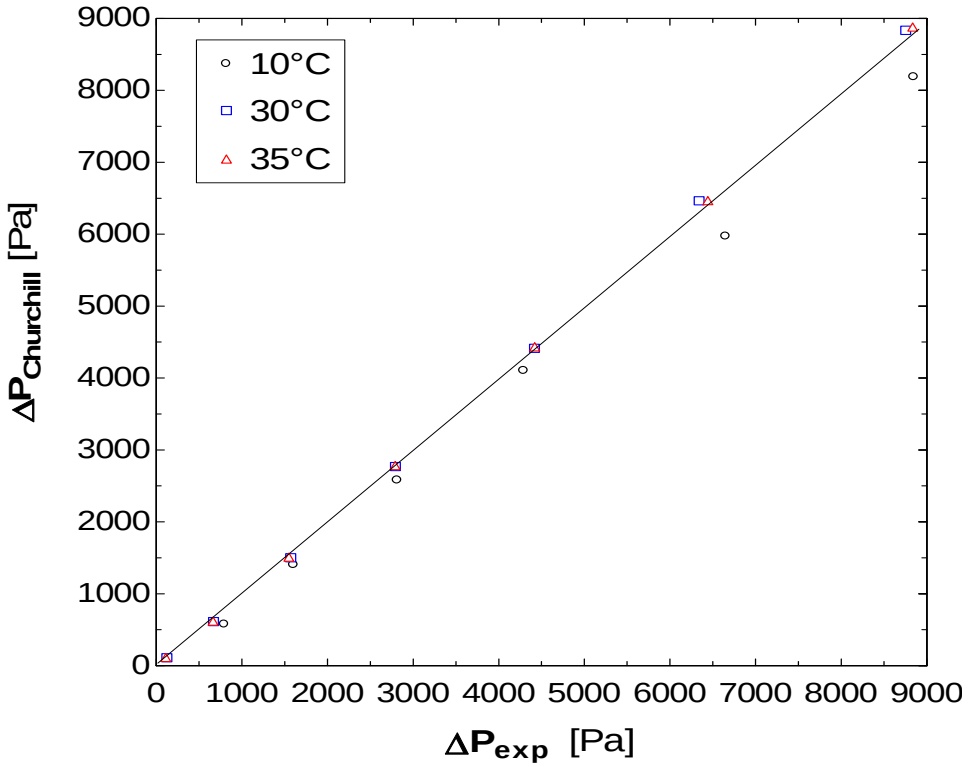

Figure 5: Single-phase pressure drop verification of the 2.92 mm flow facility

2.3 2.92 mm Facility Operation

To operate this facility, the circulating pump was first energized, then the temperature baths set to the desired operating temperature. Approximately was needed for the facility to reach the desired temperature. The desired flow rate was established by opening the flow control valves at the inlet to the test section. Pressure drop data were first obtained for single-phase liquid flow to verify that the flow and pressure transducers were functional. In addition, capacitance data were obtained at this condition for use in the capacitance scaling as described below. All fluid properties are obtained using the thermodynamic property models in EES, the Engineering Equation Solver.

The heater power was then set to obtain 5% vapor quality at the specified flow rate. After approximately 10 minutes, the pressure and temperature measurements would reach a steady state and data were acquired. This process continued in steps of 5% vapor quality until a condition of 100% vapor flow was achieved. This always occurred within one power step of the predicted power for complete evaporation. Thus, it is estimated that the uncertainty in the quality is +/- 5%. The pressure gradient and capacitance were

measured at 100% quality for verification and use in the void fraction calibration as noted below.

2.4 1.19 mm and 0.508 mm Test Setup

The virtue of the first flow facility was its thermodynamic stability. With effort, the operator could maintain exceptional temperature and mass flux stability over long operating times. For the 1.19 mm and 0.508 mm test sections, however, it became clear that the method of heating the single-phase liquid to the desired quality just could not be done with enough precision or repeatability to generate useful data for pressure drop and void fraction. Hence, a completely new approach was sought: two high-pressure syringe pumps were fabricated that allowed precise control over the flow rates of two liquid streams, one of which was completely evaporated. With this approach, the mass flux could be maintained with extreme stability and accuracy, even for very small test sections. In addition, the mass flow rate of each phase could be determined with high accuracy since the volumetric flow rate of each was known and the density could be determined through a temperature measurement.

Except for the visualization section, the entire facility was insulated using closed cell urethane foam. In order to minimize heat losses from the 1.19 mm test section, a 3/16" copper tube ran parallel to it within the insulation carrying water from a separate temperature controlled circulating bath at the desired operating temperature (30 °C or 46 °C). Temperature and pressure measurements obtained at the beginning of the pressure drop measurement were used to verify that the two-phase mixture was in saturation at the desired operating condition within the uncertainty of the pressure and temperature transducers.

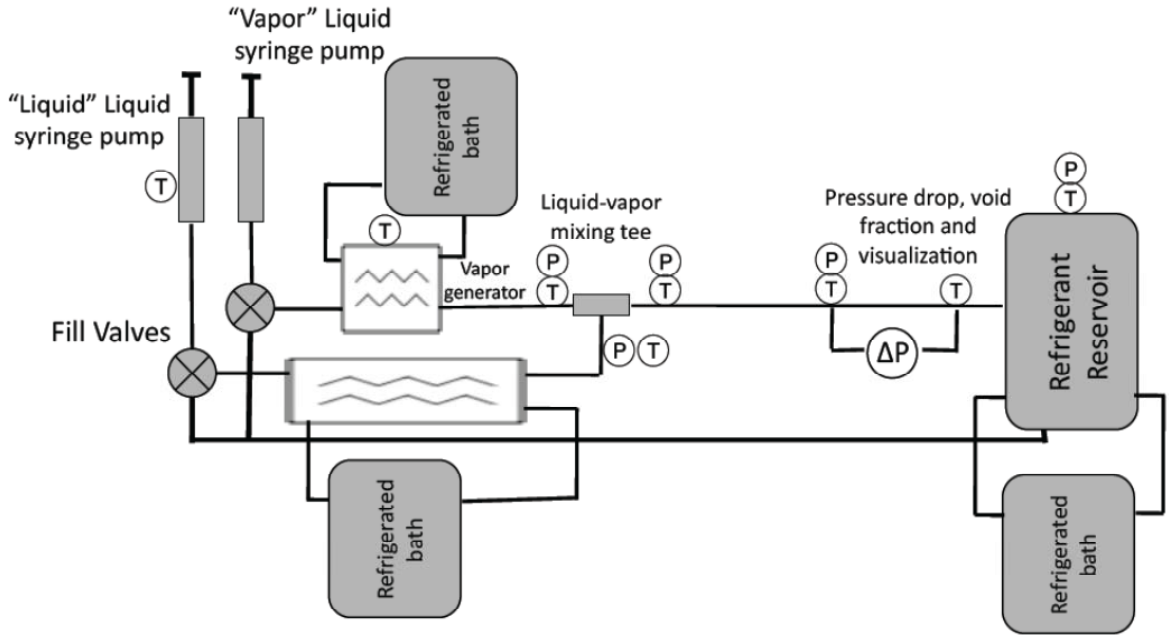

Figure 6: Schematic of flow facility for the 1.19 mm and 0.508 mm tubes.

A schematic of the flow facility is shown in Figure 6. There are five key components of the facility:

1. High pressure syringe pump set
2. Vapor generator
3. Test section for pressure drop, void fraction and visualization
4. Temperature controlled reservoir
5. Computer control system

2.4.1 High-pressure syringe pump set

The syringe pump set was custom fabricated by staff in the PIs laboratory. Design drawings can be seen in Figure 7. The core of each pump is a 50 mL stainless steel syringe rated to 600 psi from Cole-Parmer. The syringe plunger was attached via a ball joint to a plate that traversed a precision acme thread screw. Each screw was driven by a large stepper motor that received power from a micro-stepping driver. The pump was designed to drive liquid into the test section against pressures in excess of 500 psi. However, a design flaw was discovered only after the data acquisition for this project was concluded. The force transmission plate was designed to be driven by the acme thread screw via a nut fastened 25 mm above the ball joint connected to the syringe plunger. Two 12.7 mm linear bearing rods were used on either side of the plate to prevent the ensuing moment from twisting the plate out of alignment. Unfortunately, at high pressures, the moment on the plate would force the acme nut to bind and the stepper motors were not always able to overcome this additional resistance, causing them to skip steps, particularly at high rotational velocities. Thus, the actual flow rate, then, was lower than that set by the operator by an unknown amount. The screws would frequently cease to operate when the saturation temperature exceeded 46 °C, and thus the maximum saturation temperature in the test section was limited to about 46 °C.

2.4.2 Vapor Generator

The vapor generator was a simple coil-in-tube heat exchanger with hot water from a temperature controlled bath circulated through the outer tube in counter flow to the refrigerant flow through the inner coil. The coil was designed to be long enough so that the refrigerant would completely evaporate at the highest flow setting and still have a superheating length. By heating with water, the refrigerant was guaranteed to reach the same superheat temperature regardless of the flow rate, adding in maintaining the desired operating conditions.

Because the vapor enters the mixing tee slightly superheated while the liquid enters the tee slightly subcooled, the actual quality in the test section must be determined using an energy balance on the mixing tee. Temperature and absolute pressure measurements were made at both inlets and for the mixed flow at the outlet. An energy balance was performed during data post-processing to verify the quality data. If the operator made some effort to keep the vapor and liquid streams near the desired operating temperature, the mixture quality was very near to the quality calculated from the syringe pump settings (generally within 1%).

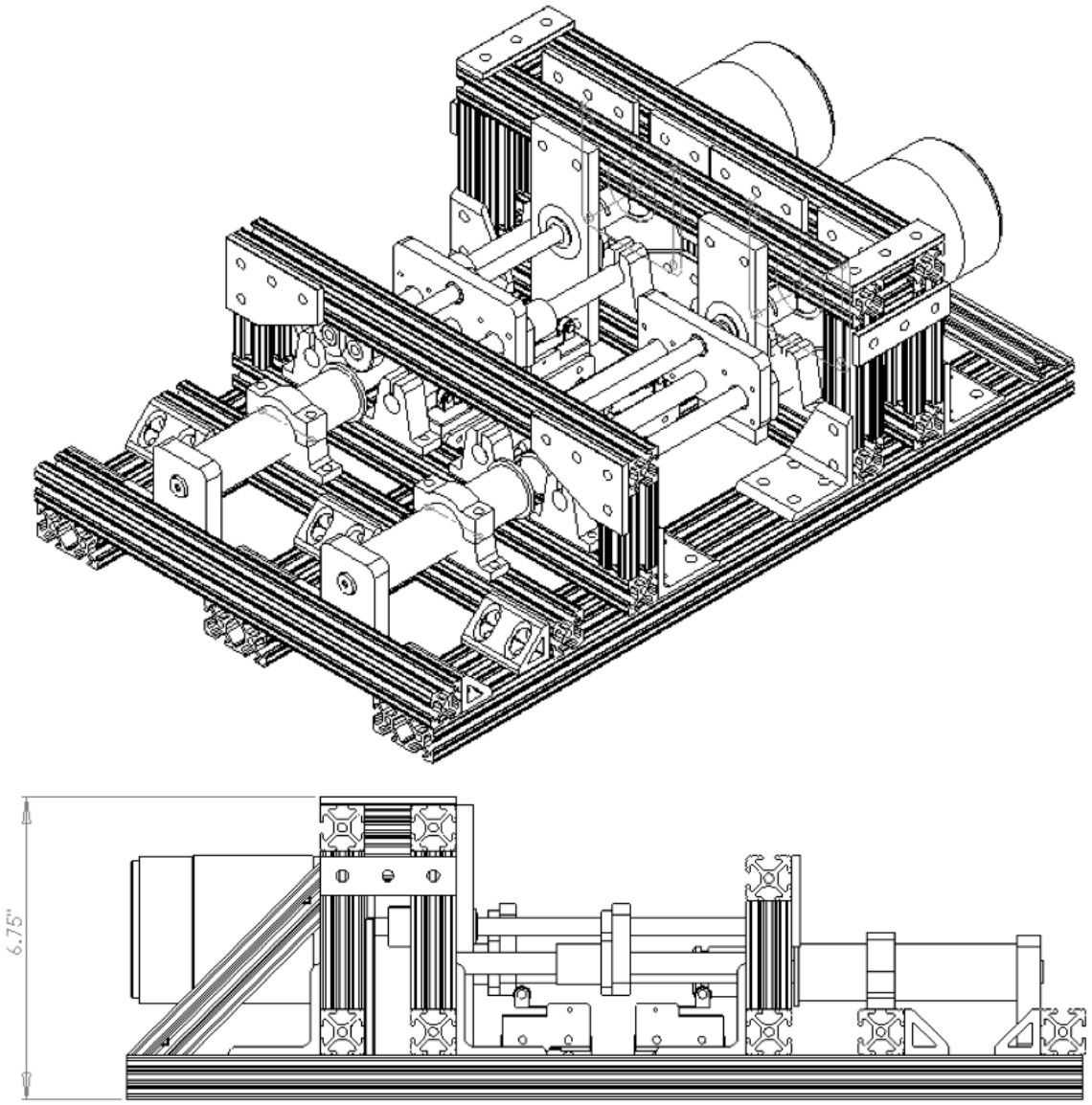

Figure 7: CAD drawing representations of the high pressure syringe pump set.

2.4.3 Test Sections

The 1.19 mm I.D. test section was fabricated from a 0.125 in. O.D. stainless steel tube. Pressure taps were formed by drilling 0.4 mm holes all the way through the test section tube. To ensure no burrs remained, the drill bit was passed through the test section from both directions, then the holes were inspected with a stereo inspection microscope. After installation, single phase liquid and vapor flows were used to verify the pressure measurement against the Churchill pressure drop correlation. As can be seen in Figure 8, the agreement between the experimental data and the correlation was quite good, within 6% mean average error (MAE).

The visualization and void fraction cannot be performed using the stainless steel test section, so a length of PTFE tubing with an I.D. of 1.05 mm was coupled to the stainless steel test section such that the misalignment was kept as small as possible. Due

to the slight difference in diameter, 100 mm of development length was provided for re-development of the two-phase flow before visualization. The void fraction measurement occurred an additional 20 mm beyond the visualization point.

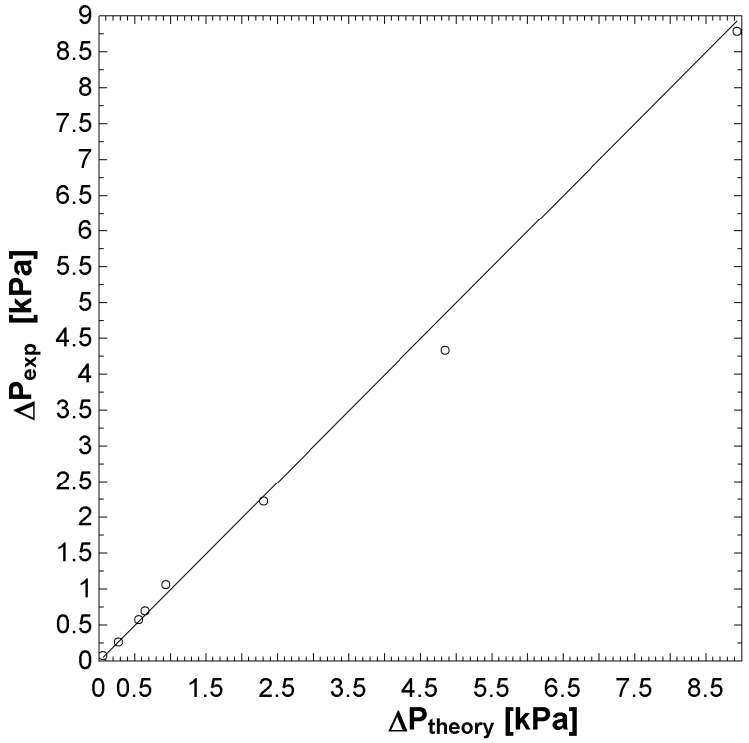

Figure 8: Single phase data points for pressure drop measurement verification for the 1.19 mm test section

The 0.508 mm I.D. test section was fabricated using a single length of ETFE (ethylene tetrafluoroethylene) tubing that had an O.D. of 0.0625 in. in order to eliminate any issues that might occur with the slight change in size from the pressure drop to the visualization and void fraction measurement sections. Fabricating clean pressure taps in this small, plastic tube proved to be very challenging, as the ability to remove material cleanly depended on the speed and feed rate of the drill or mill used, as well as the temperature of the tool and exact angle. Misalignment would easily mar the inner tube wall, as would lack of precise control of the depth of the drill bit. It was found that consistent, clean measurement port holes could be formed in the tube wall by cutting a wedge of material out of one side of the tube wall using a very sharp blade as demonstrated in Figure 9. Each wedge had an approximately 60° included angle and intersected the inner wall of the tube just enough to create a hole extending over approximately 60° of the circumference of the inner diameter. Each measurement port was then positioned entirely within a 1/16" compression fitting "Tee" that was drilled through to allow the test section tubing to slide through freely. The compression fittings were tightened at each end, sealing the measurement port. Thermocouples and pressure taps were brought in through the branch of the tee and sealed with the branch compression fitting.

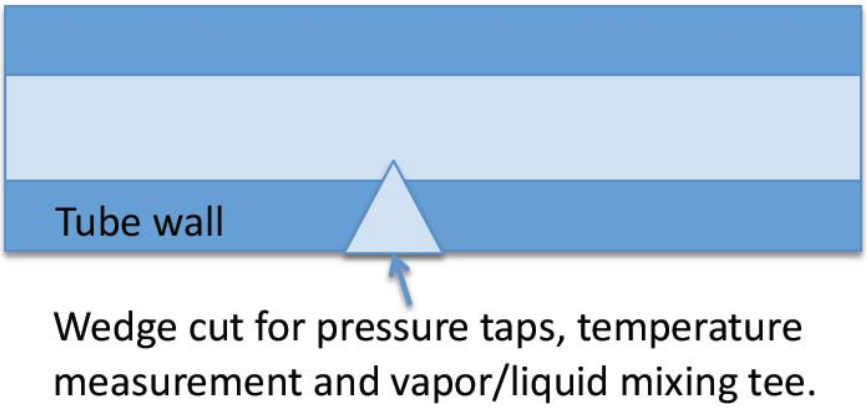

Figure 9: Schematic of the wedge configuration for measurement ports.

After installation, the test facility operation was verified with single-phase flow of liquid and vapor. The results are shown in Figure 10. As can be seen, the agreement with the Churchill correlation was excellent, within 7.5%.

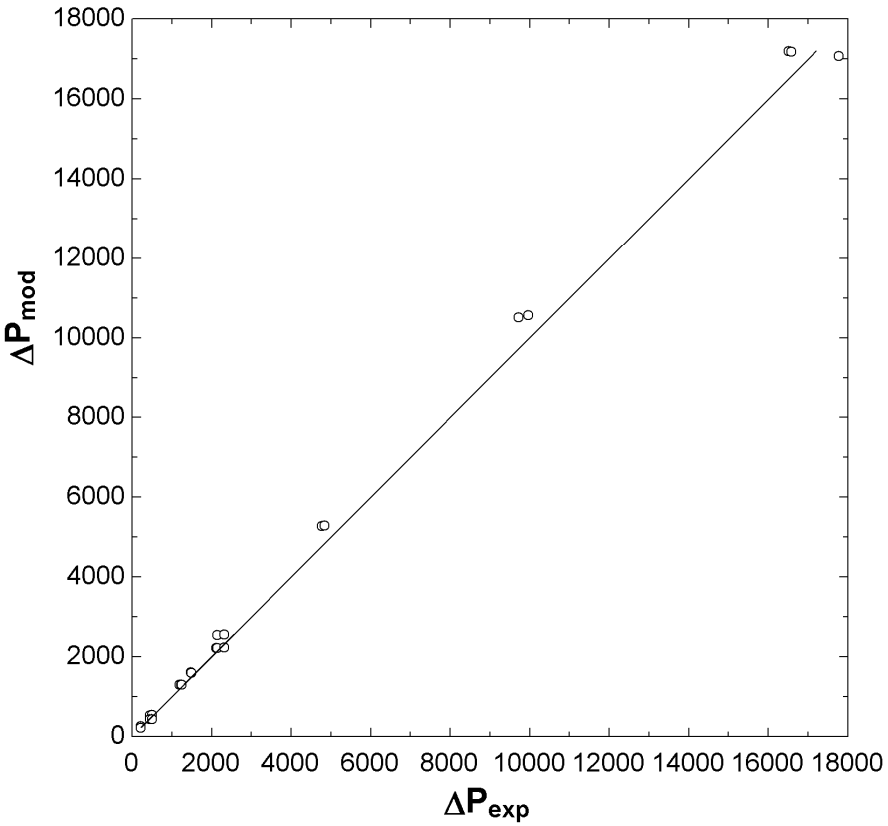

Figure 10: Test facility verification using single-phase vapor and liquid flow

2.4.4 Temperature Controlled Reservoir and Test Section

The test facility operating pressure was maintained by controlling the temperature in the refrigerant reservoir as was done with the 2.92 mm test section facility. A 1000 W

heating/750 W cooling capacity temperature controlled bath was used to set the reservoir temperature. A second, smaller temperature controlled bath was used to maintain the liquid inlet tubing and the test section support structure at the desired operating temperature. The test section was supported by a single piece of extruded aluminum framing strut (often referred to as T-slot or 80/20 aluminum extrusion) with a continuous channel along its center. Water from the second bath was pumped through the center channel of this support, which was in contact with the brass compression Tee fittings and the entire support and test section enclosed in closed-cell foam insulation. Only the visualization section remained exposed. This setup ensured adiabatic two-phase flow to the highest degree possible.

2.4.5 Computer Control

The syringe pump control and data acquisition functions were combined into a single program implemented in LabView 8.6. The user need only specify the mass flux, test section diameter and desired quality. The control program calculated the pulse frequency required to drive the stepper motors and generated the appropriate output signals that were sent to the stepper motor drivers.

2.4.6 Mixing Tee

The liquid entered the 1.19 mm test section through four holes drilled in the wall of the test section. This is an approximation to the porous wall entry considered ideal. Because of the small size of the 0.508 mm test section, the liquid is injected through one hole only. However, this hole is large enough (approximately 50% of the test section area) that the liquid momentum is low, thus mixing rapidly with the liquid. Okada and Fujita (1993) and Wolf et al. (1998) found that about 100 diameters of development length is probably required for most properties of two-phase flow to become stable in larger channels (31.4 mm I.D.). It is not known whether this same length is required for the small diameters studied here, but about 150 diameters of development length was provided for the 1.19 mm test section and about 300 diameters were used with the 0.508 mm test section. Okada and Fujita (1993) did not find a large difference in behavior between liquid injection via a jet centered in the vapor flow or a porous wall after about 300 diameters, with the porous wall liquid entry developing much sooner. Thus, it is believed that the two-phase flow in these mini-channels can be considered fully developed even though strictly porous wall injection was not employed.

2.4.7 Comments on Operation

With the 1.19 mm test section, the 800 kg m^{-2} s^{-1} condition required nearly 1 ml s^{-1} of refrigerant when running at 0% or 100% quality. Thus, the run time was limited to about 50 s. However, the system reached steady state in just a few seconds, so it was not difficult to acquire 30 s of steady state data, even at this condition. For lower flow rates and, especially, for the 0.508 mm test section, several flow conditions could be tested before recharging the pumps.

3.0 Qualitative Flow Behavior

The flow in the 2.92 mm tube behaved, on the whole, much like documented two-phase flow in larger tube diameters up to at least 19 mm. As an example, Figure 11 shows the

flow regime maps based on Thome (2008) for R-410A at 30 °C and 50 °C. Below this, Tables 2 and 3 give the observed flow regimes. It can be seen that the Thome flow regime map predicts the observed flow regimes reasonably well. Specifically, the transition between intermittent and annular flow is predicted to occur at a quality of about 0.48 for 30 °C and 0.59 for 60 °C. Except for the 200 kg m^{-2} s^{-1} data sets, these transition agree with the Wavy Annular to Annular transition noted in Tables 2 and 3.

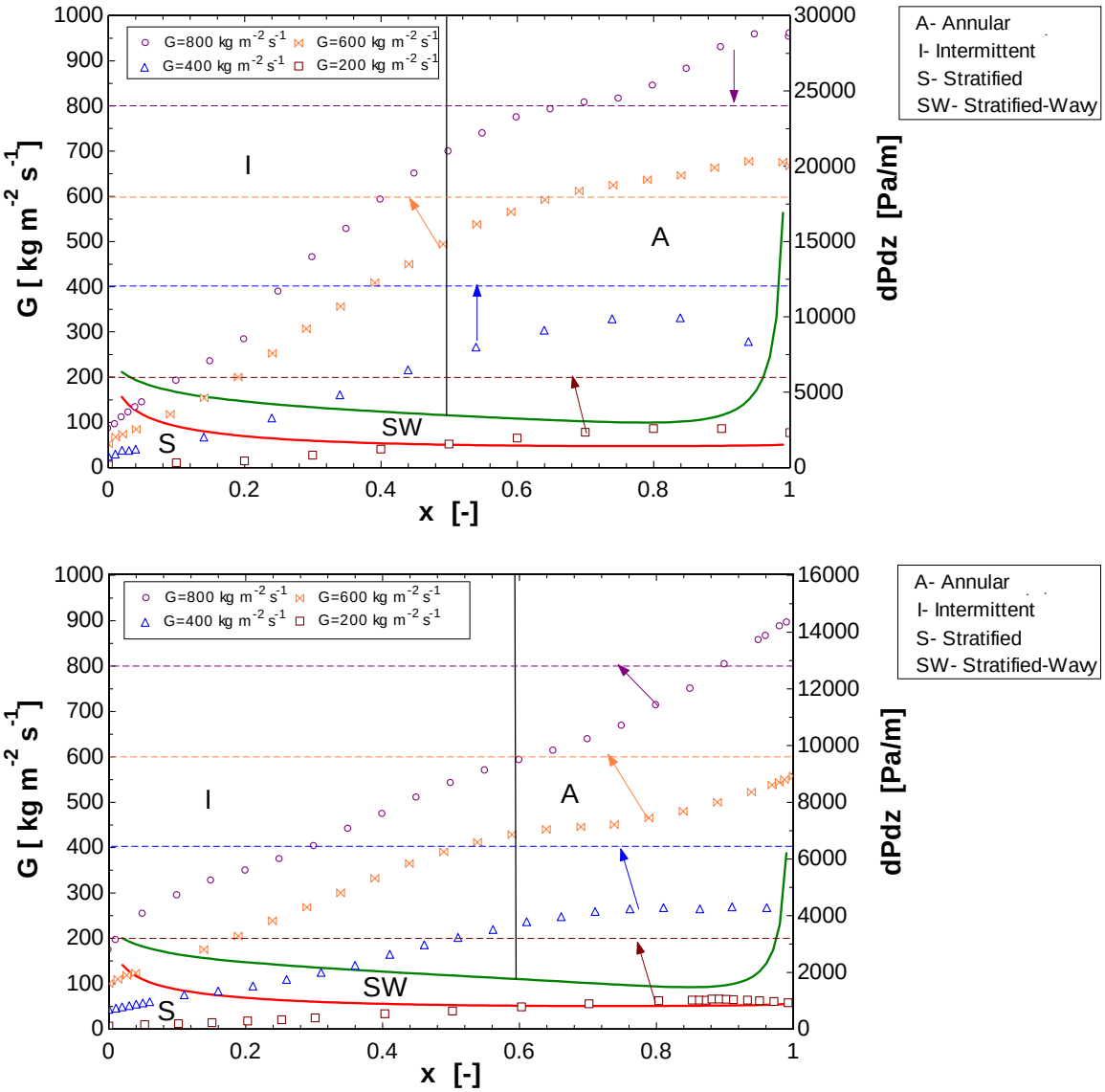

Figure 11: Flow regime maps for R-410A in the 2.92 mm tube at (top) 30 °C and (bottom) 50 °C

Table 2- Flow Regimes at T=30 °C for the 2.92 mm Tube

800 30C 3 mm		600 30C 3 mm		400 30C 3 mm		200 30C 3 mm	
x	Regime	x	Regime	x	Regime	x	Regime
0	L	0.10	STW-P	0.07	STW-P	0.22	STW-P
0.04	B-P	0.20	STW-B	0.17	STW-B	0.27	STW
0.09	B-P	0.30	WA	0.27	STW-B	0.37	STW
0.14	B-S	0.40	WA	0.37	WA	0.47	A-RW
0.24	WA-S-B	0.50	WA	0.47	WA	0.57	WA
0.34	WA	0.60	A-DW	0.57	A-DW	0.67	WA
0.44	WA	0.70	A-DW	0.67	A-DW	0.77	A-DW
0.54	A-DW	0.80	A-NW	0.77	A-NW	0.87	A-NW
0.64	A-DW	1.00	Dry	0.87	A-NW	0.97	A-NW
0.74	A-DW			0.97	A-NW		
0.84	A-NW						
0.94	A-NW						
0.99	A-NW						
1.004	Dry						

Table 3- Flow Regimes at T=50 °C for the 2.92 mm Tube

800 50C 3 mm		600 50C 3 mm		400 50C 3 mm		200 50C 3 mm	
x	Regime	x	Regime	x	Regime	x	Regime
0	L	0.07	B-P	0.06	STW-P	0	L
0.05	B-P	0.17	BS	0.16	STW-P	0.10	ST-W
0.25	WA-B	0.27	WA-B	0.26	STW-P	0.20	ST-W
0.35	WA-B	0.37	WA-B	0.36	WA-B	0.30	ST-W
0.45	WA-B	0.47	WA-B	0.46	WA-B	0.40	ST-W
0.55	WA-B	0.57	WA-B	0.56	WA	0.50	ST-W
0.65	A-DW	0.67	A-DW	0.66	WA	0.60	WA
0.75	A-NW	0.77	A-DW	0.76	A-DW	0.70	WA
0.85	A-NW	0.87	A-NW	0.86	A-NW	0.80	WA
0.95	A-NW	0.97	A-NW	0.96	A-NW	0.90	A-NW
0.98	A-NW	1.00	A-Dry	1.00	A-NW		
0.99	A-NW						

Table 4- Description of Codes for Flow Regimes

Code	Description
A-DW	Annular -Disturbance Waves
A-NW	Annular-No Waves
A-RW	Annular-Occasional Roll Waves
A-RW-S	Annular with Roll Wave and Slugs
B-P	Bubbly-Occasional Plug
BP	Bubbly Plug
B-S	Bubbly-Occasional Slug
BS	Bubbly Slug
BS-WA	Bubbly Slug-Wavy Annular
L	Liquid Phase
S-B	Slug-Bubbly
STW	Stratified Wavy
ST-W	Stratified-Occasional Waves
STW-B	Stratified Wavy-Bubbly
STW-P	Stratified Wavy-Plug
WA	Wavy Annular
WA-B	Wavy Annular-Bubbly
WA-S	Wavy Annular-Slug
WA-S-B	Wavy Annular-Slug-Bubbly

The flow in the smaller tubes is qualitatively similar to that in the 2.92 mm tube as can be seen in the attachments that present representative images of the two-phase behavior in both the 1.19 mm and 0.508 mm test sections. As can be seen, gravity continues to play a significant role in these small tubes; it is important to note at this point that all of the results presented in this work are strictly applicable only to the horizontal flow orientation. Some orientation dependence is expected.

Most striking, however, is the entrainment behavior. Note in Figures 12 and 13 how the droplets generated from the liquid are typically on the order of 100 to 200 μm in the 1.19 mm tube. Entrainment of 100 μm droplets in a tube with a diameter of 2.92 mm or larger will be important, but probably not dramatically impact the void fraction or pressure loss. However, in a 1.19 mm diameter tube, a relative few 100 μm droplets can represent a significant fraction of the total liquid flow through the tube cross-section, potentially impacting both void fraction and pressure drop. If a sufficient amount of liquid travels as droplets, the two-phase flow will begin to approximate the ideal homogeneous equilibrium mixture. This data, in fact, appear to indicate that this does occur as the tube diameter decreases.

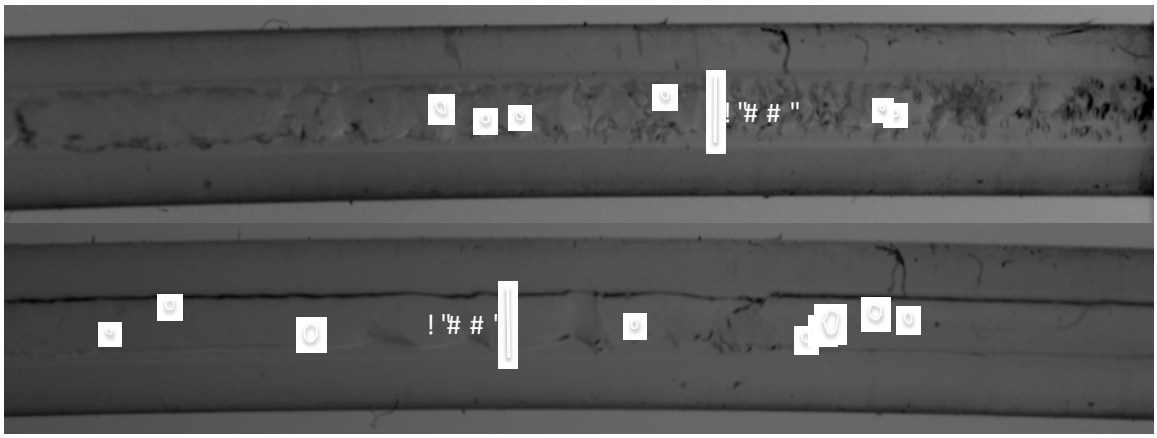

Figure 12: Examples of entrained droplets in the 1 mm visualization section during two-phase flow at significantly different conditions (600 kg/m^{2}s and 200 kg/m^{2}s)

Even more dramatic is the entrainment behavior in the 0.508 mm tube. Again, droplets on the order of 100 μm are generated from the liquid, but now these droplets occupy a significant fraction of the tube cross-section. The data presented in this report indicate that as tube diameter decreases, entrainment becomes increasingly important and directly influences both the void fraction and pressure drop.

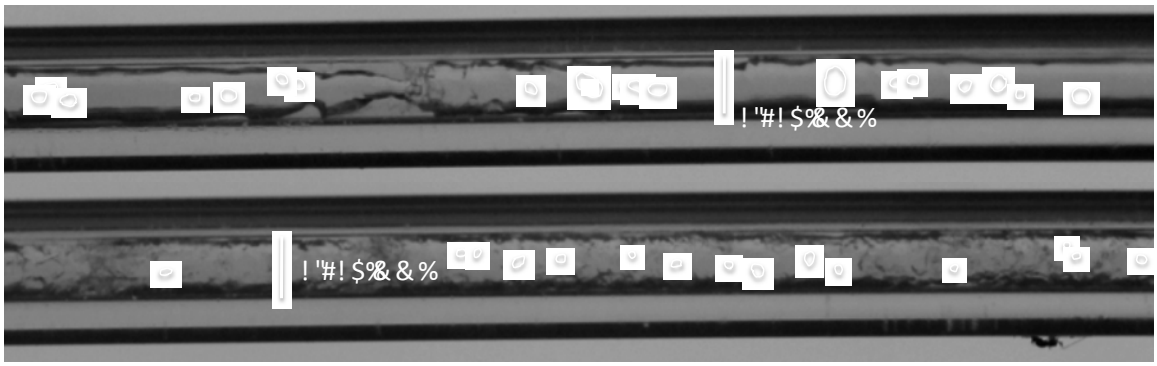

Figure 13: Examples of entrained droplets in the 0.508 mm visualization section during two-phase flow at significantly different conditions (400 kg/m^{2}s and 800 kg/m^{2}s)

Work in air-water flows in large tubes and pipes has resulted in the hypothesis that droplet diameters are directly proportional to tube diameter. This does not seem to be the case at the dimensions studied here; in the least, the droplet diameter is a weak function of diameter and a much stronger function of mass flux. It is hypothesized that, at a given mass flux, the mean vapor velocity will be approximately the same in each tube diameter, resulting in nearly identical shear behavior at the vapor-liquid interface. Thus, the forces acting to generate droplets do not scale with diameter, at least not strongly, and the droplet diameters remain relatively constant even as the tube cross-section decreases substantially.

An important hypothesis resulting from this work is that entrainment of droplets in the vapor plays a controlling role in pressure drop and void fraction in small tubes, with the effect of causing the flow to appear more homogeneous with respect to these time averaged, macroscopic measurements. The impact of this will be seen through out the remainder of the report, particularly in the modeling efforts.

4.0 Pressure Gradients

4.1 Pressure Gradient: 2.92 mm

The pressure drop data for the 2.92 mm tube are presented in Figure 14. The solid lines represent predictions from a new model based on that of Müller-Steinhagen and Heck (1986) that is derived below. The 800 kg/m^{2}s data at 30 °C do not have the generally expected curve with respect to *x*, especially at higher qualities. It is hypothesized that this is due primarily to the inability of the evaporator to reach a steady state condition at the highest mass flux and quality. This effect is seen at 600 kg/m^{2}s as well, though much less pronounced. This is consistent with an incomplete heating. The test facility was unable to generate reliable data at 800 kg/m^{2}s and 50 °C.

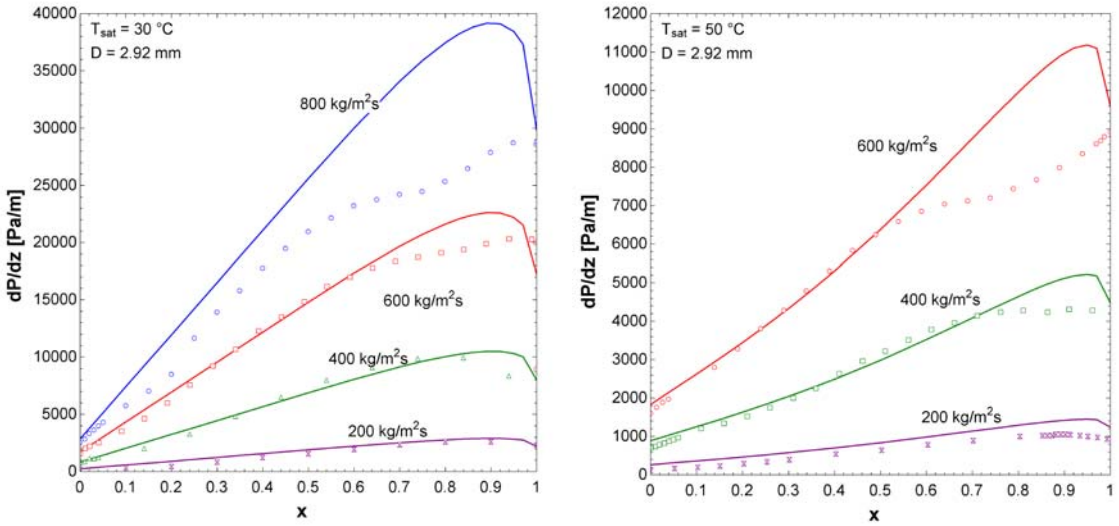

Figure 14: Pressure drop data for R 410A flowing through a 2.92 mm I.D. tube at two different saturation temperatures. Note that different scales are used to allow for easier visualization of the data.

4.2 Pressure Gradient: 1.19 mm

The pressure gradient data for flow through a 1.19 mm tube are presented in Figure 15. The data obtained at a saturation temperature of 32 °C tend to be lower than the new model predicts. It is not clear whether this discrepancy is due to an issue with the experimental setup or with the modeling approach. Given that the data do not approach the expected pressure gradient as the quality approaches 1, it is likely that the experimental setup was not providing the desired operating conditions throughout the

entire range of flows. The 50 °C data are generally within the expected range of pressure loss.

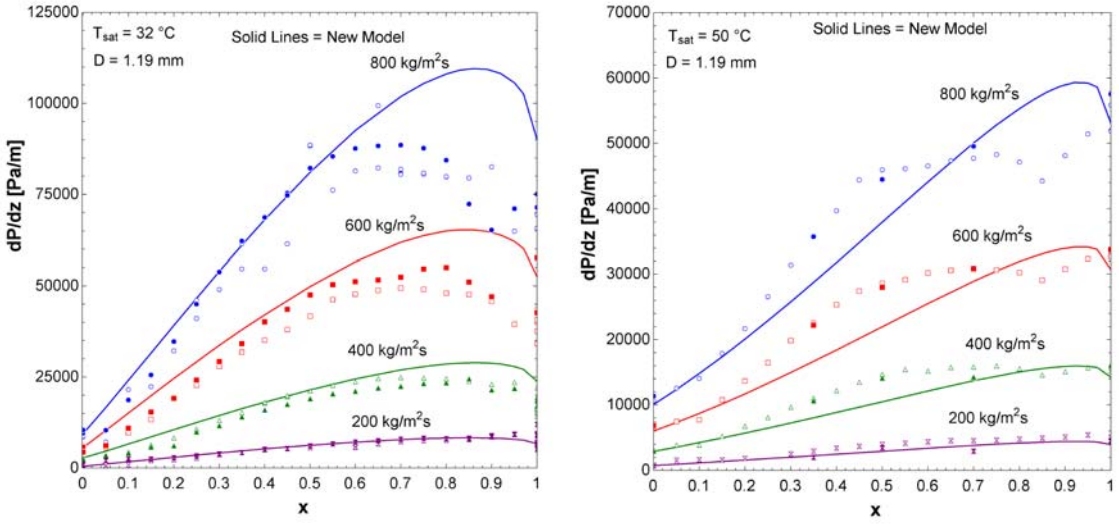

Figure 15: Pressure gradient data for R410A flowing through a 1.19 mm tube at two different saturation temperatures. Note that different scales are used to allow for easier visualization of data. Solid symbols indicate data obtained to verify repeatability.

An important observation is that these data, and those following for the 0.508 mm tube, indicate that the peak in the pressure gradient *does not correspond to a dryout condition* as is frequently hypothesized. This may be easily verified by reviewing the images from the flow visualization attached to this report. In fact, the peak in pressure gradient is related to the disappearance of relatively large wave structures at the liquid/vapor interface, consistent with the findings of McDermott (2008) for R-123 flowing in a 19 mm pipe. Further, this is strongly consistent with the local shear measurements obtained in air-water flow by Ashwood (2010) using micro-PIV. These indicated that wave structures contribute to the overall shear independently from the liquid film in between them; once the wave structures disappear, a significant source of shear disappears as well. The mechanics of wave generation and dissipation, however, are still open questions for further study.

4.3 Pressure Gradient: 0.508 mm tube

The pressure gradient behavior of R-410A two-phase flow in a 0.508 mm tube is shown in Figure 16. The data are generally quite clean. At the highest temperature, the syringe pump stepper motors would occasionally stall. Several attempts were made to correct this behavior, but it appears that the 800 kg/m^{2}s flow could not be maintained.

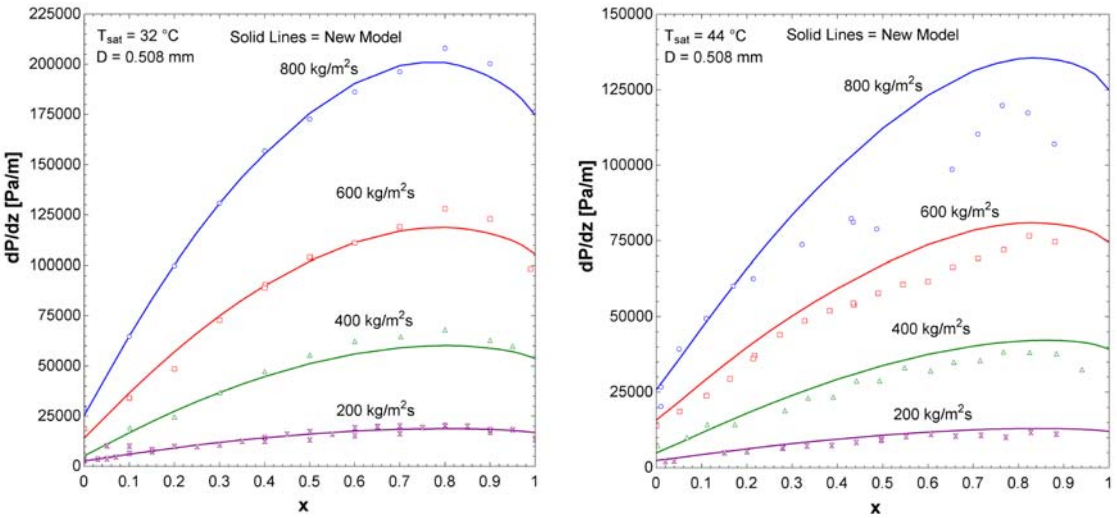

Figure 16: Pressure gradient data for R410A flowing through a 0.508 mm tube at two different saturation temperatures. Note that different scales are used to allow for easier visualization of data.

5.0 Comparison with Pressure Gradient Models

Pressure drop in conventional channels have been actively studied for many years, with widely used correlations dating back to the 1940's, such as the classical Lockhart and Martinelli (1949) correlation. Currently, two-phase pressure drop models can be essentially categorized as 1) two-phase multiplier, 2) phenomenological, 3) empirical curve fit or 4) flow-regime based.

The two-phase multiplier is among the most popular of these classes, with the Lockhart-Martinelli correlation, derived from work presented by Martinelli and Nelson (1948), serving as a foundation for many. Grönnerud (1979) developed a two-phase multiplier correlation specifically for refrigerants including the liquid Froude number and is applicable to vapor qualities from $0 \leq x < 1$. About the same time, Friedel (1979) developed a modified two phase multiplier correlation based on a data bank of 25,000 points for adiabatic flow through channels with $D_h > 1$ mm and Hewitt et al. (1994) recommended it for cases when surface tension data are available. Zhang and Webb (2001) simplified Friedel's correlation significantly by relying on the reduced pressure (P/P_{crit}) rather than other dimensionless groups. Cavallini et al. (2002) proposed a modified Friedel model for the frictional pressure gradient for a wide range of refrigerants including R-410A during condensation at 30 and 50 °C and mass velocities varying from 100 to 750 kg/m^{2}s in an 8 mm I.D. tube over the entire quality range. The Zhang and Webb (2001) correlation was used for comparison with the current data set and found to predict pressure gradient with a mean absolute error of 20.8 %.

Chisholm (1973) provided a theoretical foundation for the Lockhart-Martinelli correlation with the inclusion of an additional parameter that has been adopted by several researchers working with mini- and micro-channels. Mishima and Hibiki (1996) applied this model to air-water flow in mini-channels with good success. Qu and Mudawar (2003) studied hydrodynamic instability and pressure drop in a water cooled two-phase sink containing 21 parallel 231 x 713 μm microchannels. They modified the Mishima and Hibiki (1996) correlation by incorporating a mass velocity term. The correlation proposed yielded a MAE of 12.4% in their study. Later, Field and Hrnjak (2007) made further modifications to the Chisholm correlation based on the work of Lee and Lee (2001) and Suo and Griffith (1964). Unfortunately, these models are not valid near the limits of very high and very low quality and they significantly underpredict the current data.

Phenomenological models are those that attempt to model key physical behaviors with analytical expressions and empirical data as needed. They tend to be made up of a significant number of equations that need to be solved numerically, and as such are not generally widely adopted for design work. Some examples of this type of model for two-phase flow include Hurlburt and Newell (2000), Fukano (1995), Schubring and Shedd (2010). Other models are strongly rooted in a physical theory, though simplified enough to be calculated relatively easily.

Another common class of phenomenological models are those that are modifications to the Homogeneous Equilibrium Model. These include Chen et al. (2002) who developed an empirical correlation modifying the homogenous model based on a bank of 1484 data points for air-water and several refrigerants including R410a for $D <$ 10 mm reinforcing the importance of surface tension in small tubes compared to gravitational force including a Bond number and a Weber number. A modification of the homogeneous model was proposed by Wang et al. (2001) that includes the effect of surface tension through the introduction of the Bond number. When compared to the present data set, the Chen model predicted pressure gradient to within 22.8 % mean absolute error, but the Wang et al. model consistently gave excessively low predictions.

Revellin and Thome (2006) obtained two-phase pressure drop data for microchannels of 0.509 and 0.790 mm I.D. for two refrigerants R-134a and R-245fa and proposed a modification of the homogeneous model using the two-phase friction factor. This new model applies to turbulent flow with a two-phase Reynolds number of less than or equal to 8000 and it was developed with a least square method. Possibly because the current data set includes many data that are not in the applicable range of the correlation, the Revellin and Thome correlation significantly over predicts the current data.

The most successful of the purely empirical approaches is the correlation by Müller-Steinhagen and Heck (1986). They constructed their correlation by first setting the output to the pure liquid or vapor values as appropriate. Based on very limited empirical observations, they then assumed that the lower quality data could be modeled as essentially linear, with the pressure gradient at a quality of 0.5 equal to the pressure gradient of pure vapor. Finally, they combined they combined this linear behavior with the fixed value of the all vapor pressure drop using a power law asymptotic matching with an exponent of 3. Although the correlation is simple and the assumptions made in its derivation very big, the correlation predicts the current data set to within 20.5% mean absolute error.

6.0 A New Pressure Drop Correlation

The Müller-Steinhagen and Heck (1986) correlation has been shown by increasing numbers of studies to predict the pressure gradient in adiabatic two-phase flow remarkably well. As shown above, it reproduces the current data to within ±20.5% with no alteration. Upon closer inspection, however, it becomes apparent that the correlation is increasingly inaccurate as the tube size decreases and the saturation temperature rises. Under these conditions, the pressure gradient profile as a function of quality becomes less peaked in the higher qualities and the slope of pressure gradient versus quality approaches 1 in the lower qualities. The Müller-Steinhagen and Heck correlation is re-stated here for convenience:

$$\left.\frac{dp}{dz}\right|_{f\,2\phi} = \Lambda(1-x)^{1/n} + \left.\frac{dp}{dz}\right|_{go} x^n \tag{3}$$

$$\Lambda = \left.\frac{dp}{dz}\right|_{lo} + m\left(\left.\frac{dp}{dz}\right|_{go} - \left.\frac{dp}{dz}\right|_{lo}\right)x \tag{4}$$

$$\left.\frac{dp}{dz}\right|_{lo} = f_l \frac{2G^2}{\rho_l D}, \left.\frac{dp}{dz}\right|_{go} = f_g \frac{2G^2}{\rho_g D} \tag{5}$$

$$f_l = \frac{0.079}{\mathrm{Re}_l^{0.25}}, f_g = \frac{0.079}{\mathrm{Re}_g^{0.25}} \tag{6}$$

$$\mathrm{Re}_l = \frac{GD}{\mu_l}, \mathrm{Re}_g = \frac{GD}{\mu_g} \tag{7}$$

where $m = 2$ and $n = 3$.

Although the original correlation was derived as essentially a curve fit based on a few general assumptions, it actually captures a significant amount of physical behavior. First, the endpoints at x = 0 and 1 correctly reach the appropriate single phase limits. However, as originally formulated, the correlation assumes smooth-walled tubes and turbulent flow (Re > 10000). Single-phase flow measurements in the current test sections indicated that the walls were not always smooth, and the Re is frequently under 10000, especially on the liquid side. To improve on the correlation, then, the Churchill correlation is used to determine the all liquid and all vapor pressure gradients. This correlation smoothly transitions from turbulent to laminar flow and takes into account rough-walled tubes:

$$f = 8\left[\left(\frac{8}{\mathrm{Re}}\right)^{12} + \left(\left[2.457\ln\left(\frac{1}{\left(\frac{7}{\mathrm{Re}}\right)^{0.9} + 0.27RR}\right)\right]^{16} + \left(\frac{37530}{\mathrm{Re}}\right)^{16}\right)^{-1.5}\right]^{1/12} \tag{8}$$

Next, the value *m* in Equation (4) controls the slope from x = 0. If *m* = 1, then the increase in the pressure gradient from x = 0 would be linear with quality, *x*, and suggests that each phase is in contact proportionally to its mass fraction and that the total friction is made up of the linear contribution of each phase. Thus, *m* captures the nature of the friction between the phases, conceptually similar to the two-phase interaction parameter of Chisholm (1967). *m* should have a lower bound of 1, consistent with a purely homogeneous two-phase flow with non-interacting phases. Based on the predictive ability of the original correlation, it appears that *m* has an upper bound of 2, but there is not a clear physical constraint that would require this. Physically, m = 2 dictates that the magnitude of the maximum in the pressure gradient versus x profile would be equal to the liquid pressure gradient plus twice the difference between the liquid and vapor pressure gradients at the same mass flux.

Through analysis of the current data set, it was observed that *m* is primarily a function of the saturation temperature. However, it is more likely that this is a reflection of the fact that the fluid properties are strong functions of temperature. Considering the idea that the slope is related to the interaction between the phases, it is hypothesized that the slope is actually a function of the density ratio as well as other factors that limit it to values between 1 and 2. In the absence of knowledge about these other factors, a polynomial least squares fit was generated to cause *m* to vary appropriately between 1 and 2.

$$m = 1.9638 + 7.1698 r_\rho - 180.38 r_\rho^2 + 887.88 r_\rho^3 - 1823.0 r_\rho^4 + 1687.0 r_\rho^5 - 579.63 r_\rho^6 \qquad (9)$$

where r_ρ is the ratio of the vapor to liquid densities.

The exponent in the power law combining scheme essentially controls the location and height of the peak in the pressure gradient curve. Its lower limit must be 1 for the combination to remain physical while its upper limit appears to be 3, though there is no physical rationale for this. The data from the current experiment indicate that the exponent is a strong function of the tube diameter and a weak function of temperature. Further, it is hypothesized that the important geometrical factor is the ratio of the diameter to the capillary length, or the length over which surface tension holds strong influence. The capillary length is defined as

$$\lambda = \sqrt{\frac{\sigma}{\rho_l g}} \qquad (10)$$

where σ is the surface tension, ρ_l is the liquid density and *g* is the acceleration due to gravity. An equation was found through trial and error that gives the correct general behavior of *n* for the range of data studied, and should extend to other refrigerants as well:

$$n = 3 - 2\left(1 - \left[\exp\left(-\lambda/D\right)\right]^2\right) \qquad (11)$$

The modified Muller-Steinhagen and Heck correlation is compared with the current data set in Figures 14 through 16 above. It predicts the data to within 17.2% mean absolute error. Although this MAE is not significantly better than the original

correlation, it seems to represent the physics of the problem better. In this case, it seems to capture the trends that the flow approaches homogeneous behavior at high saturation temperatures (i.e., as the density of the vapor increases relative to the liquid) and as the tube diameter becomes smaller. Four correlations that predict the data well are compared in Figure 17 versus the experimental data. Note that these correlations represent three different approaches: modified Friedel, which is itself a two-phase multiplier approach, a modified homogeneous model and a purely empirical correlation. The fact that these three disparate approaches all predict the data well attests to the general quality of the data, even though some issues with the data acquisition and facility operation were discussed in the results section.

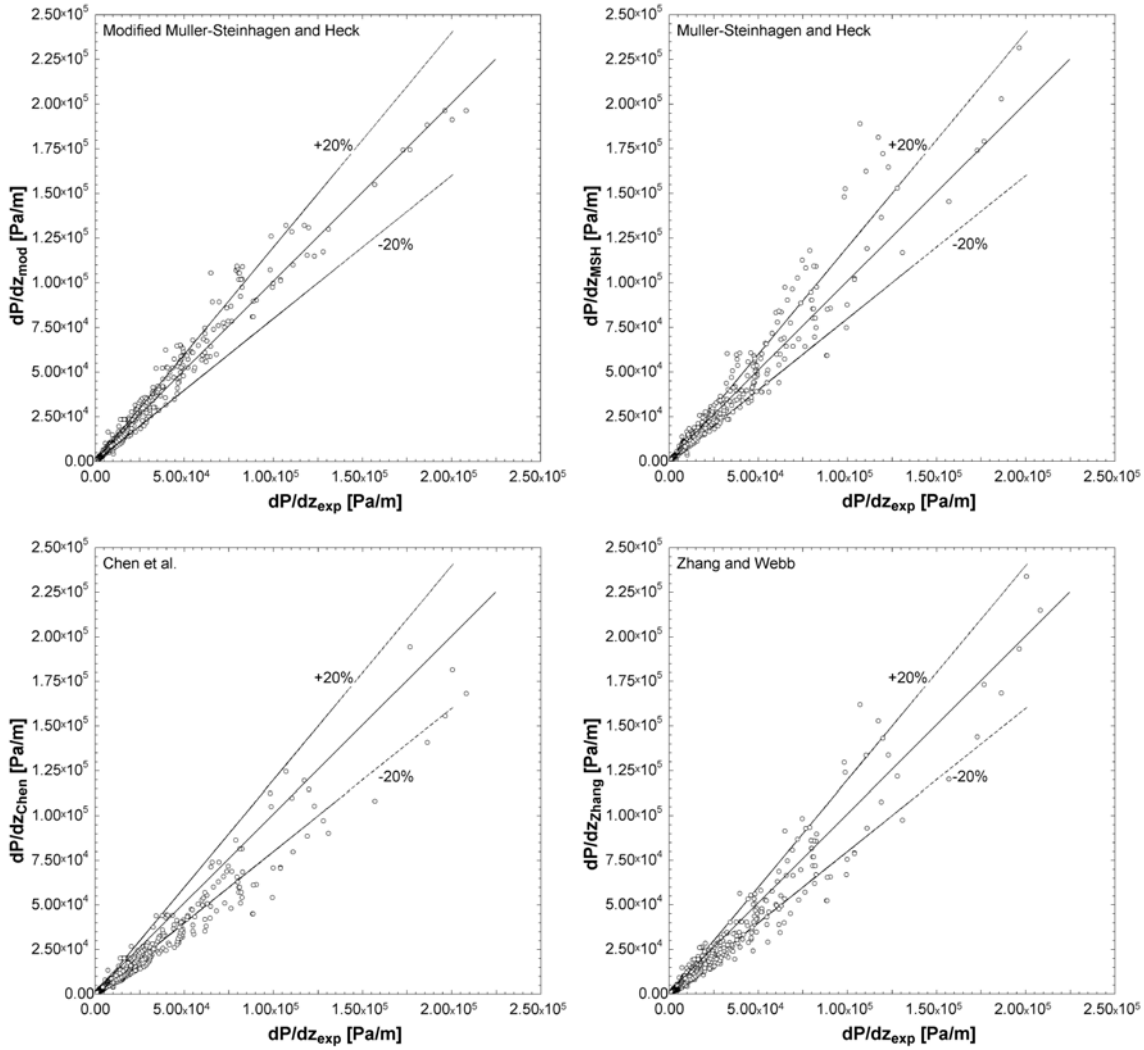

Figure 17: Performance of four empirical and semi-empirical correlations for pressure gradient.

7.0 Void Fraction Measurement

7.1 Experimental Background

Knowledge of the void fraction of a two-phase flow can be an extremely powerful tool for the modeling pressure drop and heat transfer coefficients in two-phase flow applications, including heat exchangers used in coal, gas, and nuclear power generation systems, the piping systems in the oil and gas industry, steam generators, and chemical reactors. Turbulence, phase slip, and compressibility, among other issues complicate two-phase flow models, but in order to accurately design these systems, it is necessary to identify the relationships between two-phase flow regimes and corresponding pressure drop and heat transfer coefficients.

Unfortunately, accurate means of measuring void fraction are limited, particularly in mini and micro-channels. Hewitt (1978) cites a number of possible techniques to measure void fraction depending on whether volumetric, cross-sectional averaged, chordal averaged or local measurements are desired. Thome in the Wolverine Tube Inc. Engineering Data Book III (2006) describes the various geometric definitions for specifying the void fraction in great detail. These will be described in this work based on his descriptions.

Local void fraction refers to a measurement at a point or very small volume; when liquid only is present, the void fraction is equal to 0 and when vapor only is present, it is equal to 1. The chordal void fraction is usually measured by directing a narrow beam of radiation through a channel with a two-phase flow inside. It requires the calibration of the absorption rates for the vapor and liquid phases. The intensity of the beam on the opposite side of the test section can be measured, from which the fractional length of the path through the channel occupied by the vapor phase can be determined.

The volumetric void fraction is typically measured by means of quick closing valves installed along the channel. A two-phase flow is first established, and then the valves are activated and trap the two-phase fluid. The respective vapor and liquid volumes are determined by draining the liquid or by weighing the test section. Cross sectional void fraction is typically obtained by optical means or by an indirect non-intrusive approach such as the capacitance of the mixture. It is also mentioned by Thome (2006) that cross sectional void fraction is the most widely used definition of void fraction.

Perhaps the easiest method of actually measuring void fraction to implement is the quick-closing valve method, though several experimental difficulties exist even with this. The method relies on simultaneously operated valves at either end of a test section that close rapidly, trapping vapor and liquid in the channel. With care, the liquid can be drained and its volume measured, giving a measure of the volume occupied by the liquid at the instant that the valves closed. Quick closing valves have been found to provide very repeatable results in a wide variety of experiments ranging from large tubes using air and water to multiport minichannels using R410A (Niño et al., 2002). In fact, this method is frequently used as a reference by which other systems are calibrated.

For experiments in very small channels using refrigerants at condensation conditions, however, the quick closing valve system presents numerous challenges. Further complicating things, if the data need to be obtained for flow at an elevated temperature, the test section would need to be maintained at exactly the test conditions

while liquid is transferred and measured. The transfer of liquid is problematic because of the role of surface tension in retaining liquid in the channel. While draining the microchannel, a thin film of liquid may be left behind. This may not be significant in larger pipes, but a 20 micron film on the wall of a 500 micron diameter channel represents an 85% void fraction. Vapor will rapidly condense or liquid will rapidly evaporate with slight changes to the environmental conditions. Thus, the quick closing valve method is not at all suitable for many applications with pure fluids in small channels, either as a measurement option or as a calibration technique.

Serizawa et al. (2002) measured void fraction in microchannels by means of high speed video pictures, assuming symmetrical shape of bubbles and gas slugs, and the void fraction obtained correlated well with the Armand (1946) correlation with some scatter in their data. This study only concerns bubbly and slug flow. Recent published work by Kawahara et al. (2002), and Chung and Kawaji (2004) suggests that void fractions measured using images of flow through micro-scale round tubes could have uncertainties in the range of 0.05 to 0.01. This, however, cannot be possible without careful refractive index matching and high-resolution optics (see, for example, Rodriguez, 2004, and Fukamachi et al., 2003). Based on the reported resolution of the imaging system used by Chung and Kawaji (2004), the uncertainty could have been no better than 0.15, excluding significant errors that would result from the lensing of the curved tube walls. Thus, direct imaging of flow in microchannels cannot be used to measure accurate void fractions.

Mishima and Hibiki (1996) measured void fraction with the use of neutron radiography and image processing techniques. A neutron beam, which penetrated horizontally across a vertical upward air-water flow in an aluminum test section, was attenuated in proportion to the thickness of the water layer along its path. The image could be observed in real time and void fraction was obtained by measuring the brightness of the video images. Their void fraction data correlated well with the drift flux model.

Some additional methods include radiation attenuation that can be expensive and from a safety stand point difficult to implement; electrical resistance probes which disturb the flow field and are not applicable to refrigerants, and the impedance technique using capacitance sensors. The capacitance sensor technique is preferred over resistance probes due to their non-intrusive nature of measuring void fraction and the fact that they are relatively simple and inexpensive to implement compared to other techniques. Within the impedance technique there are different configurations of the sensors, such as concave plate, helically coiled, and the ring type that are among the most commonly used in the literature.

Compared to the helically coiled configuration, which requires strategic shielding to prevent edge effects and stray capacitance, the ring type sensors are most suitable to implement, since the shielding to prevent stray capacitance is easier to achieve according to Pawlosky et al. (2004). Furthermore, it was found by Elkow and Rezkallah (1996) that the problems associated with the helical type sensors, such as the non-linear response, poor sensitivity, and poor shielding, can be eliminated using the concave-type sensors as mentioned by Ahmed (2006). In addition, Ahmed (2006) proved that the ring-type sensors, as well as the concave-type, provide a linear relationship between capacitance and void fraction, with the only difference that the ring-type sensor provides a higher sensitivity than the concave-type for the same spatial resolution.

Thus, a capacitance sensor seems to be among the best and most appropriate choices for the measurement of void fraction in mini- and micro-channels. The calibration of the sensor remains a significant issue, however. In previous implementations, the capacitive sensors have been calibrated using phantoms, which are solid forms intended to represent different void fractions within the tube and are usually made of polymers that have similar dielectric constants as the fluids being studied as shown in Pawlosky et al. (2004).

However, this method can be very inaccurate if the phantoms are ill-fitting in the test section and if their dimensions are not known very precisely. In addition, phantoms cannot duplicate the dielectric constants of refrigerants that vary dramatically from fluid to fluid as well as with the temperature of the fluid. Furthermore, Ahmed (2006) presents a correlation between void fraction and normalized capacitance by applying a linear regression to the capacitance data of the ring type sensor. This calibration is given by

$$\varepsilon = 0.756 C_n \tag{12}$$

By definition, the normalized capacitance ranges from 0 to 1, so, strangely this calibration returns a maximum value of 75.6% void fraction for a maximum value of a normalized capacitance of unity, when a normalized capacitance of unity void fraction should by unity as well. This may have occurred because Ahmed may have been concerned only with low values of void fraction.

7.2 New Calibration Procedure

A new calibration procedure to measure void fraction by means of capacitance using the ring-type sensor by forcing homogeneous flow to occur in a rigid flow loop is proposed. In homogeneous flow, the slip between the vapor and the liquid goes to zero, and the void fraction can be found from knowledge of the volume occupied by each phase in the loop. It was found that, using this technique, a single relationship between the normalized capacitance of the sensor and the void fraction could be found. This calibration is then applied to capacitance data from R-410A refrigerant flowing through a 3 mm, and 1 mm nominal I.D. horizontal tube at 30 °C and 50 °C.

7.2.1 Sensor construction

The ring sensor includes two sets of electrodes. The electrodes for the 2.96 mm test section were constructed of four 2 mm wide, 0.1 mm thick copper strips. The strips were wrapped around the 6 mm O.D. test section quartz tubing with the ends extending in alternating directions. According to Ahmed (2006), the sensitivity of the ring sensor is maximized by minimizing the electrode spacing to below at least 2 mm. In this case, the copper strips were placed 1 mm apart. The copper strip ends were soldered to two BNC cable wires as demonstrated in Figure 18. Then, the BNC cables were then connected to the Boonton 72-B capacitance meter. Stray capacitance and electrical noise were limited by a metal shield surrounding ring-type sensors.

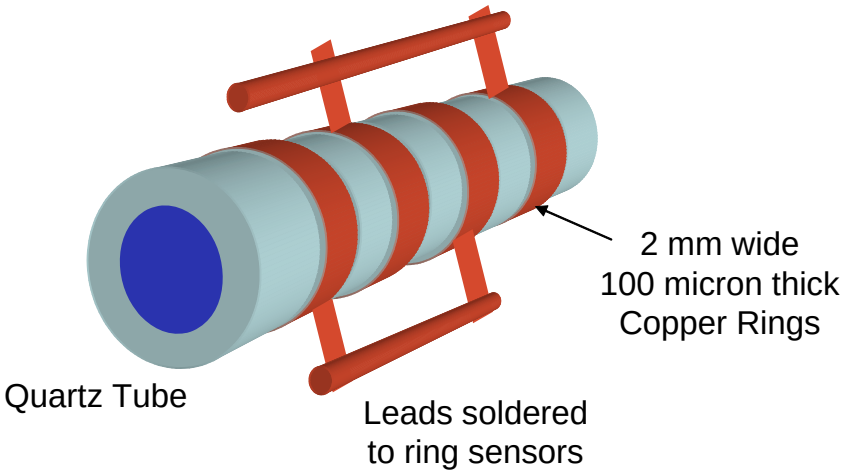

Figure 18: Sketch of the ring capacitance sensor used for the 2.92 mm test section.

In preparation for rebuilding the test facility for the 1.19 mm test section with the syringe pumps, a series of finite element simulations were carried out on the electrode configurations. These simulations indicated that the consistency of the void fraction signal could be significantly improved by adding grounded guard rings on either side of the capacitor electrodes. Thus, the sensor configuration for the 1.19 mm and 0.508 mm test sections was constructed as shown in Figure 19. The finite element simulations also showed that while non-uniform distribution of the vapor and liquid could impact the void fraction reading, the impact was not very significant due to the ring sensor geometry. In addition, the average void fraction remained very consistent if the distribution of vapor and liquid varied somewhat with time, as is the case in the two-phase flows observed in this project.

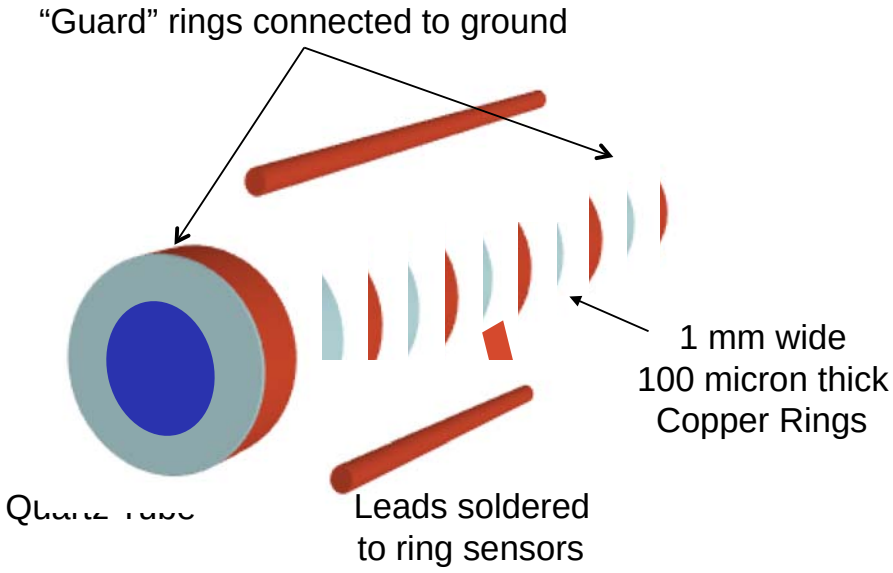

Figure 19: Sketch of the void fraction sensor used for the 1.19 mm and 0.508 mm diameter test sections.

7.2.2 Calibration flow loop

A flow loop, shown in Figure 20, was designed to be rigid at low pressure, consisting of a peristaltic pump from Cole-Parmer with variable speed and direction, a 15 cm length of Masterflex precision tubing (only where the pump is engaged), and a 3 mm and 1 mm I.D. quartz test section with the ring sensors described above, depending on the case being studied. The remaining tubing in the loop was made of semi-rigid polyethylene tubing with 1.25 mm thick walls, providing a rigid channel at the pressures at the near atmospheric pressures where the calibration was performed. A pair of syringes connected to 3-way valves was used to change the volume fraction of the two-phase mixture in the loop. The Boonton 72B capacitance meter with an accuracy of ±4% in the 10 pF range was used to obtain the capacitance measurements.

The capacitance meter generates an analog voltage signal proportional to the capacitance value, which is collected via a National Instruments PCI 6024E multifunction data acquisition module. Lab View 8.0 is used to control the data acquisition and to collect and record data. A virtual instrument (VI) was created to record data.

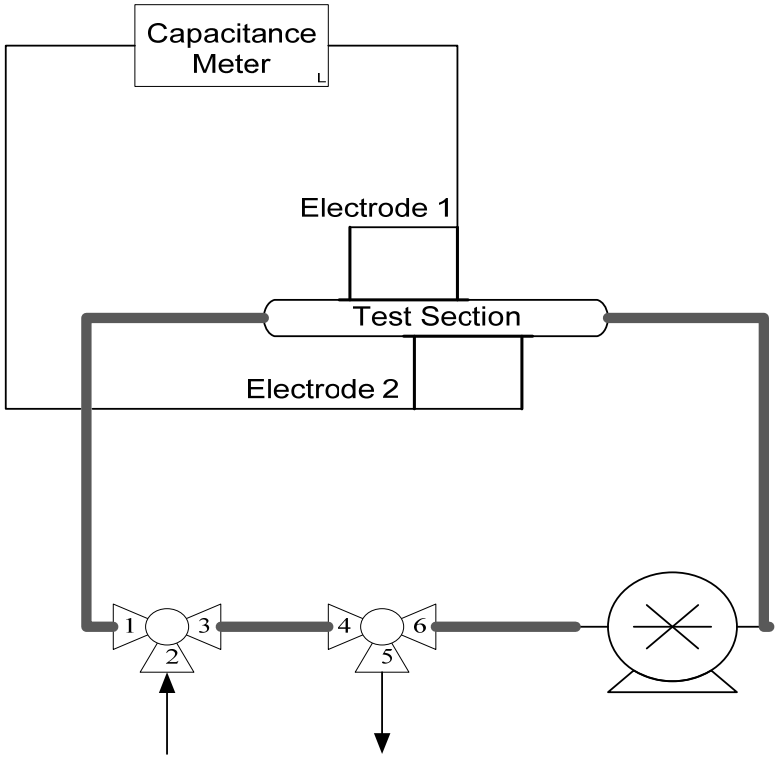

Figure 20: Void fraction sensor calibration flow loop.

7.2.3 Calibration

In order to relate a capacitance sensor reading to the corresponding void fraction, the sensor must be calibrated for various known void fractions. In general, this is very difficult to do. However, if a two-phase mixture flows through a test facility of constant volume, then liquid may be added while the same volume of gas is removed to set a known volumetric fraction of liquid in the facility. A pump that can handle two-phase flow may then be used to move the gas and liquid around the facility and through the

void fraction sensor. If a long time average is taken, the mean signal from the sensor will represent the time averaged volume fraction of gas in the facility. This is the basis of the novel void fraction calibration being presented.

The calibration technique proposed was tested in the rigid flow loop shown in Figure 20 for ethyl alcohol as the liquid part of the two-phase flow and air as the gas. The total volume of the loop was determined to be 37.2 mL by filling the loop with 100% pure ethyl alcohol, emptying it and measuring the volume of liquid. The peristaltic pump, once engaged, displaces a certain volume, measured to be 0.4 mL, changing the overall volume of the loop. To account for this, 0.4 mL of fluid was removed from the loop before the beginning of a series of tests using a syringe via port 5 on the right hand 3-way valve in Figure 20 after the pump was engaged, providing a total volume of 36.8 mL in the flow loop.

The calibration was performed in 6 different ways. The first test began with the flow loop filled with liquid at a moderate pump speed. Capacitance measurements were recorded for 60 seconds to obtain a sufficient number of data points to take an average making sure that a reliable number is obtained at each void fraction change. The capacitance sensor was sampled at 10 kHz, and then every 1000 points were averaged to remove high frequency noise. Approximately, 600 capacitance values were written to a file for each void fraction. These were then averaged, so a total of approximately 600000 data points were used for each void fraction measurement.

After the 100% liquid data were obtained, the pump is unclamped so that fluid can move freely through the flexible tubing, and ports 3 and 4 are closed. Then, a syringe was used to remove 3.7 mL of liquid via port 2. Simultaneously, 3.7 mL of air was added to the loop using a syringe via port 5. The pump was re-engaged and, after about 30 seconds, data acquisition commenced.

The process was repeated until all of the liquid had been removed and replaced with air. The process was then repeated starting with all air and ending with all liquid. These emptying and filling procedures were repeated for a total of 3 pump velocities and two pump directions to verify that there were no bias or hysteresis errors in the procedure. All of the capacitance data points were normalized according to Equation (13):

$$C_n = \frac{C_l - C_m}{C_l - C_v} \tag{13}$$

where C_n is the normalized capacitance ranging from 0 to 1, C_l is the 100% liquid capacitance, C_v is the 100% gas capacitance and Cm is the measured two-phase capacitance.

The data from all of the calibration runs are plotted as Void Fraction versus C_n in Figure 21. A direct curve fit of these data suggested a third order polynomial, but it included an offset that was not physical. Thus, the following third order polynomial was found that meets the correct end criteria and matches the mid-void fraction data very well.

$$\varepsilon = C_n^3 - KC_n^2 + KC_n \tag{14}$$

where K is a parameter that adjusts the calibration curve for variations in dielectric constants

$$K = 0.0056\kappa + 2.2 \tag{15}$$

The data near zero in Figure 21 are prone to large relative error due to small errors in extracting or adding fluid to the calibration facility. In order to validate the new void fraction calibration, data for different fluids with a wide range of dielectric constants (see Table 5) were used to calibrate the void fraction conversion curve and the resulting correlation is quite good. This was done for channels with 3 mm and 1 mm I.D.

In order to use Equation (14) to calculate void fraction for R-410A, a modification to the K parameter has to be made in order to account for the temperature dependence of the dielectric constant of the refrigerant.

$$\kappa = 69.0 - 0.314T_{sat} + 0.000379T_{sat}^2 \tag{16}$$

Equation (16) is a curve fit to data from Brito et al. (2000) for the dielectric constant of R-410A at lower pressures.

Validation of the general calibration that relates normalized capacitance to void fraction is necessary. Figure 22 shows void fraction data using the proposed calibration for PF-5060 and FC-40 with 3.8% and 5.8% MAE respectively.

Table 5-Fluids Used to Validate Calibration

Fluid	Dielectric Constant
Water	70
Ethyl-Alcohol	24
PF-5060	1.75
FC-40	1.9
HFE-7100	7.4
Ethylene Glycol	37.4

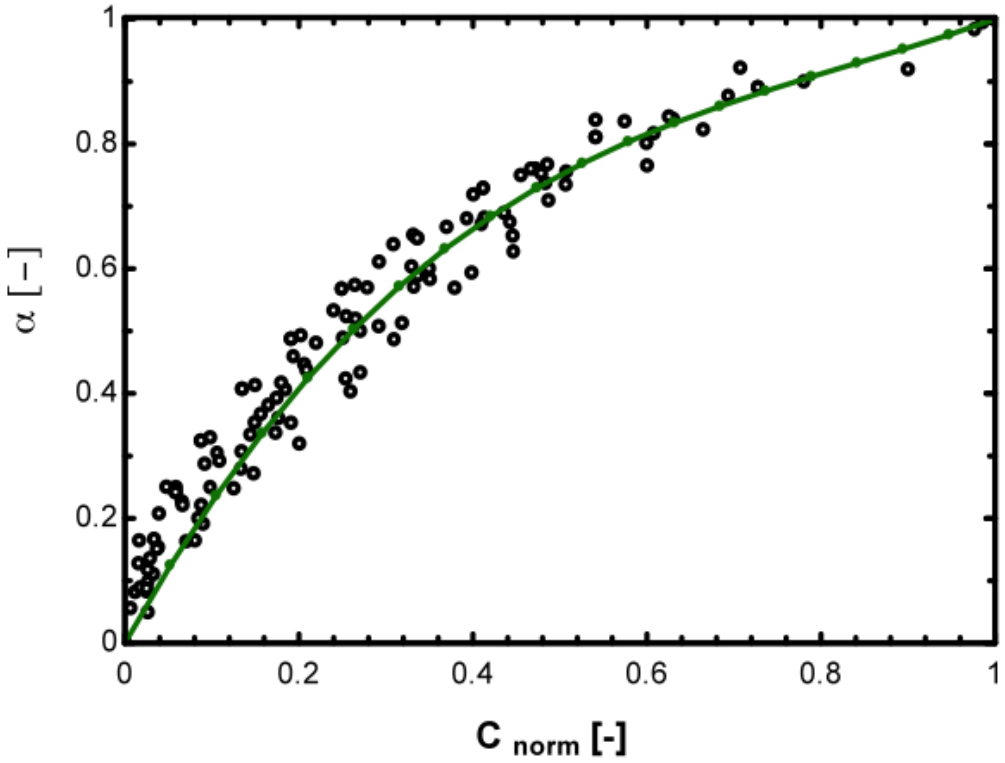

Figure 21: Calibration results using ethyl alcohol in the 3 mm and 1 mm test loops.

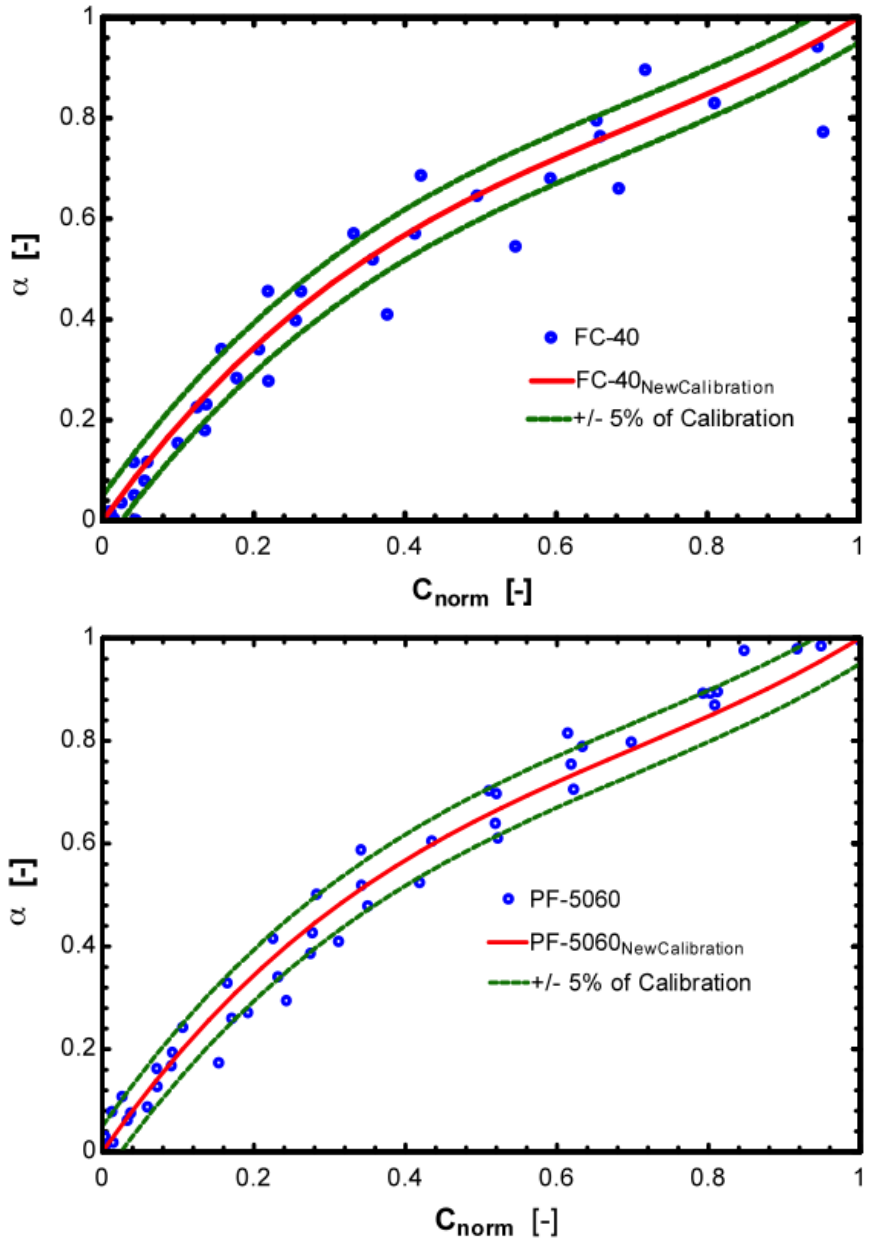

Figure 22: Validation tests in the calibration facility using FC-40 and PF-5060.

8.0 Void Fraction Results

8.1 Void Fraction: 2.92 mm tube

The results of the void fraction measurement in the 2.92 mm test section are shown in Figures 23 and 24. Each plot presents the data along with the predictions of three models, discussed in detail below. The Homogeneous Equilibrium Model represents the maximum void fraction for a given quality that can exist in concurrent two-phase flow. This is because, in homogeneous flow, the vapor will flow at the lowest velocity possible for a given mass flow. (Again, this statement is not necessarily true if counter current flow is present on average.) The highest possible vapor velocity will occur in separated flow where the vapor does not interact with the liquid. However, this is not a realistic case, as a large relative velocity between the phases will generate interfacial instabilities, leading to interaction between the phases. A separated flow model that has been shown by a number of studies to be accurate for two-phase flow in larger diameters is that of Rouhani and Axelsson. The new model shown in the plots is a weighted combination of these two.

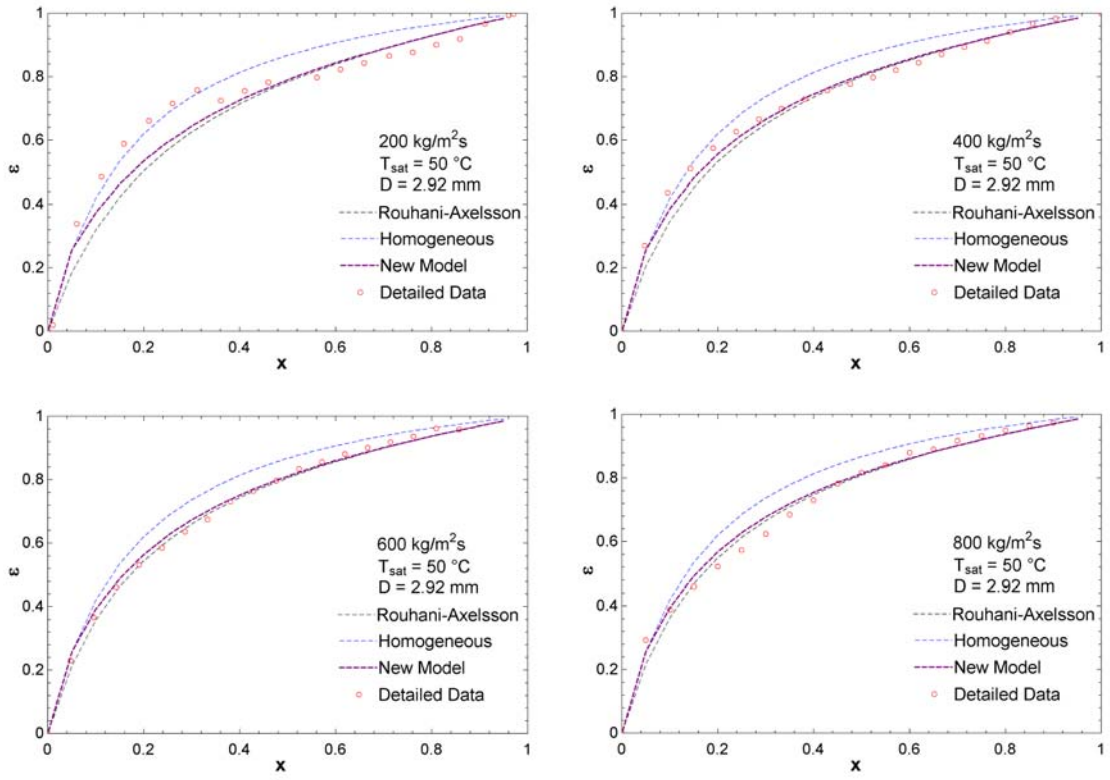

Figure 23: Void Fraction data compared with models for a 2.92 mm I.D. tube with T_{sat} = 50 °C.

First, comparing the 30 °C and 50 °C saturation temperature data, it is clear that the higher saturation temperature has a more gradual growth in void fraction as a function of quality as compared with the lower temperature data. This trend is due to the significantly higher density of the vapor at 50 °C (139 kg/m^3 vs. 76 kg/m^3). The denser

vapor requires less space at the same mass flux, so the void fraction will be lower at the same quality.

The data at both temperatures tend to follow the Rouhani-Axelsson model of void fraction. There seems to be a trend with mass flux of the data moving from the left to the right of the model, but more data are needed to confirm this trend. A behavior that is demonstrated more clearly in the data is that of the tendency of low-quality data to follow the homogeneous model before transitioning to the Rouhani-Axelsson behavior. This transition tends to begin at the point that vapor penetrates the liquid slugs completely.

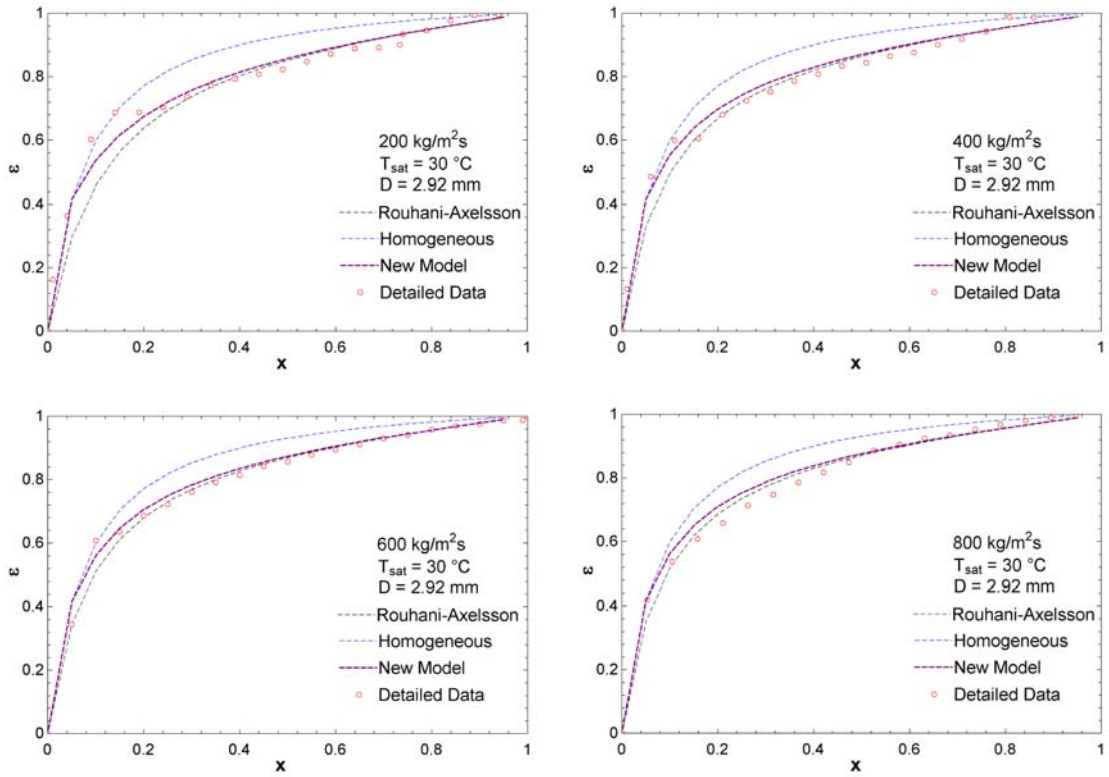

Figure 24: Void Fraction data compared with models for a 2.92 mm I.D. tube with T_{sat} = 30 °C.

8.2 Void Fraction: 1.19 mm tube

The data for the 1.19 mm tube, shown in Figures 25 and 26, are again bracketed by the Homogeneous and Rouhani-Axelsson models of void fraction. It is now clearer that the data start out at low qualities following the homogeneous model, beginning a gradual transition to the Rouhani-Axelsson behavior between 10% and 20% quality. This transition from homogeneous to separated flow behavior is much more pronounced in the 1.19 mm tube than in the 2.92 mm tube.

As discussed above, this gradual transition may be explained by the entrainment behavior observed in the two-phase flow. The average size of the liquid droplets entrained from the waves does not seem to scale with the diameter. Thus, at lower qualities where the two phase flow contains relatively large waves, a significant volume of the test section will be occupied by large (relative to the diameter) liquid droplets that

flow with a velocity similar to the vapor. The relative importance of these droplets decreases with increasing quality.

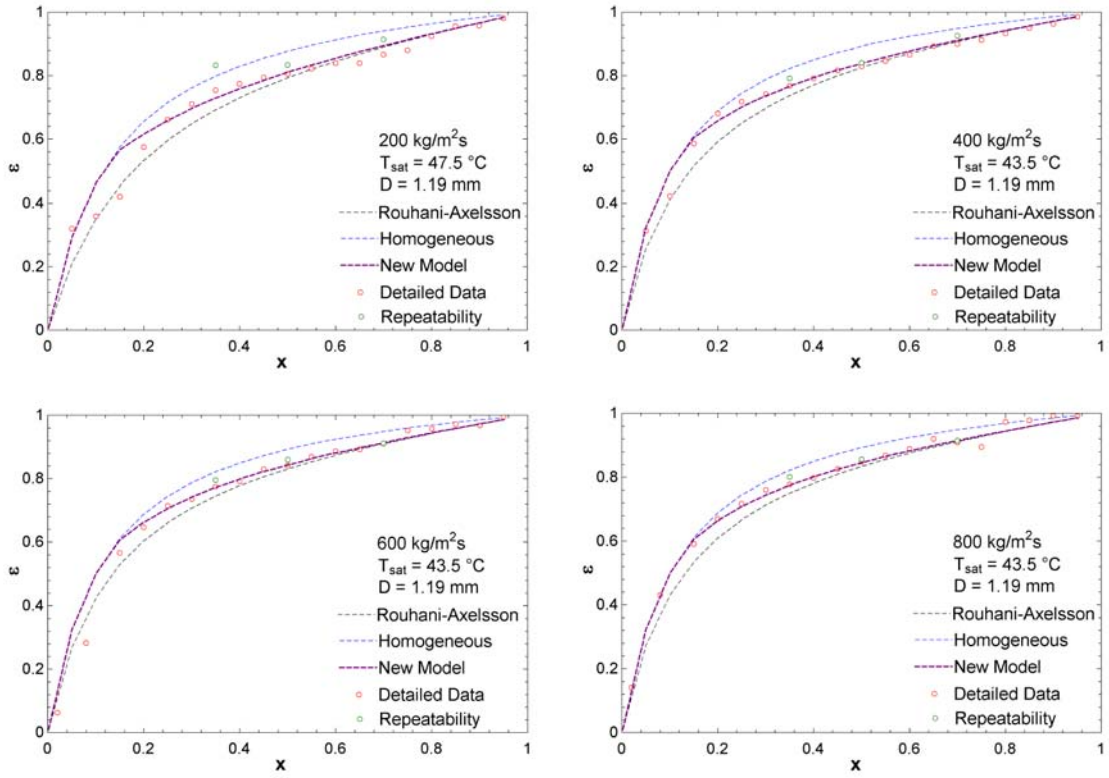

Figure 25: Void Fraction data compared with models for a 1.19 mm I.D. tube with T_{sat} approx. 44 °C.

Repeatability data are included on these plots. The repeatability is generally quite good, though in some cases there are large deviations. The true uncertainty in the data is difficult to determine. The standard deviation of the capacitance signal was within 1% to 2%, while the standard error, a more accurate measure of the uncertainty in a large data set, was smaller by about an order of magnitude. However, this is only one part of the entire uncertainty, which includes the ability to repeat the flow condition and test section temperatures exactly, and the calibration curve. A better worst case estimate of the uncertainty is about 5% across the entire range from 0 to 1, with the uncertainty generally higher at the low void fractions and smaller at the high ones.

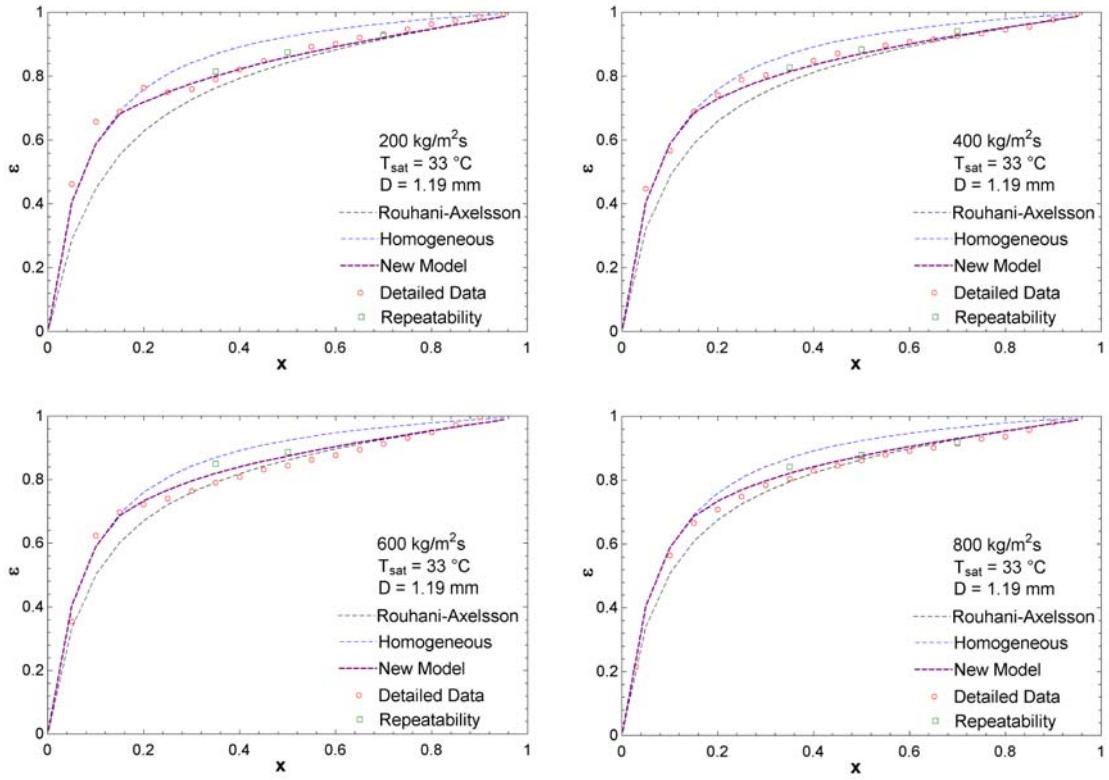

Figure 26: Void Fraction data compared with models for a 1.19 mm I.D. tube with T_{sat} approx. 33 °C.

It is very important to note that in both the 1.19 mm and 0.508 mm void fraction data, the transition between the homogeneous curve and the Rouhani-Axelsson curve takes place essentially during the time that significant droplet entrainment can be observed in the tube. Entrainment begins at approximately the point where the liquid slugs are pierced by advancing vapor, which is the point of divergence between the data and the homogeneous curve. Once entrainment decreases to nearly zero, the void fraction appears to align with the Rouhani-Axelsson model. Thus, it appears that the unique void fraction behavior of microchannel two-phase flow may be directly, and completely, determined by droplet entrainment.

8.3 Void Fraction: 0.508 mm tube

Although somewhat noisier, the data in Figures 27 and 28 show that the behaviors observed in the larger tubes continue into the smallest one. The trends with temperature are consistent across all tube sizes while the void fraction in the 0.508 mm tube follows the homogeneous equilibrium model to higher qualities than occurred in the 1.19 mm tube. The repeatability data indicate generally good consistency, though some runs deviate by more than 5%. As noted with the pressure drop data, there were some difficulties in maintaining consistent flow rates as the syringe pump worked to overcome both pressure and friction forces.

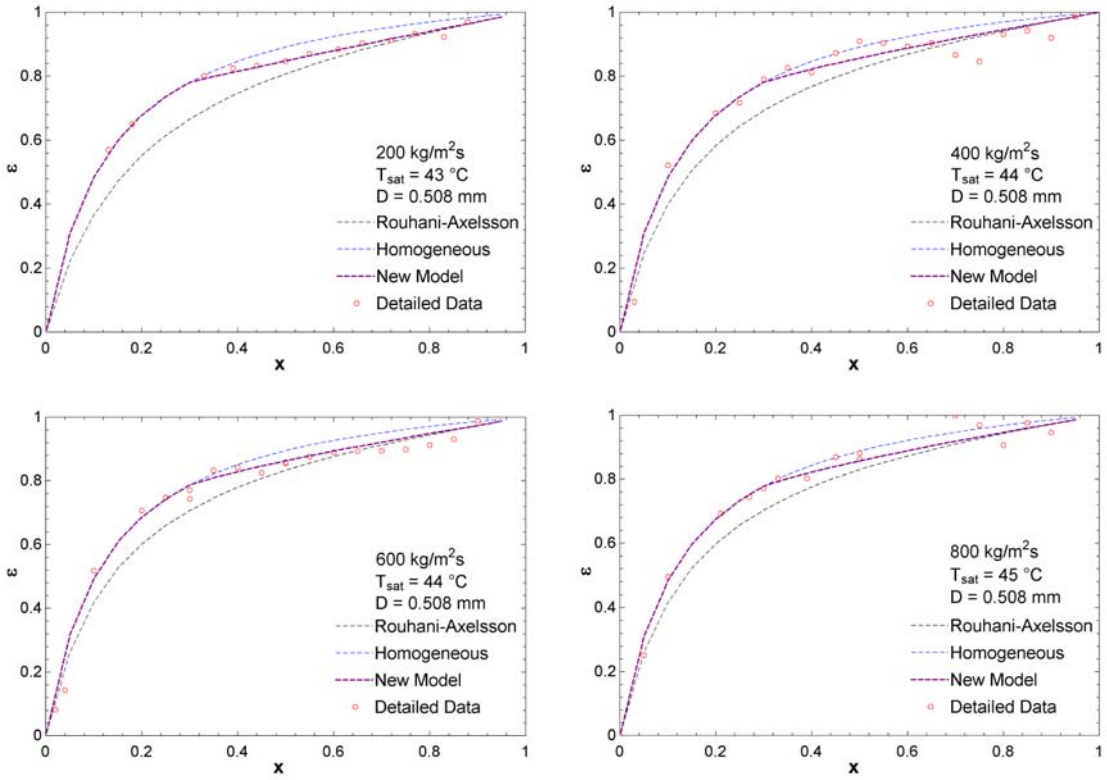

Figure 27: Void Fraction data compared with models for a 0.508 mm I.D. tube with T_{sat} approx. 44 °C.

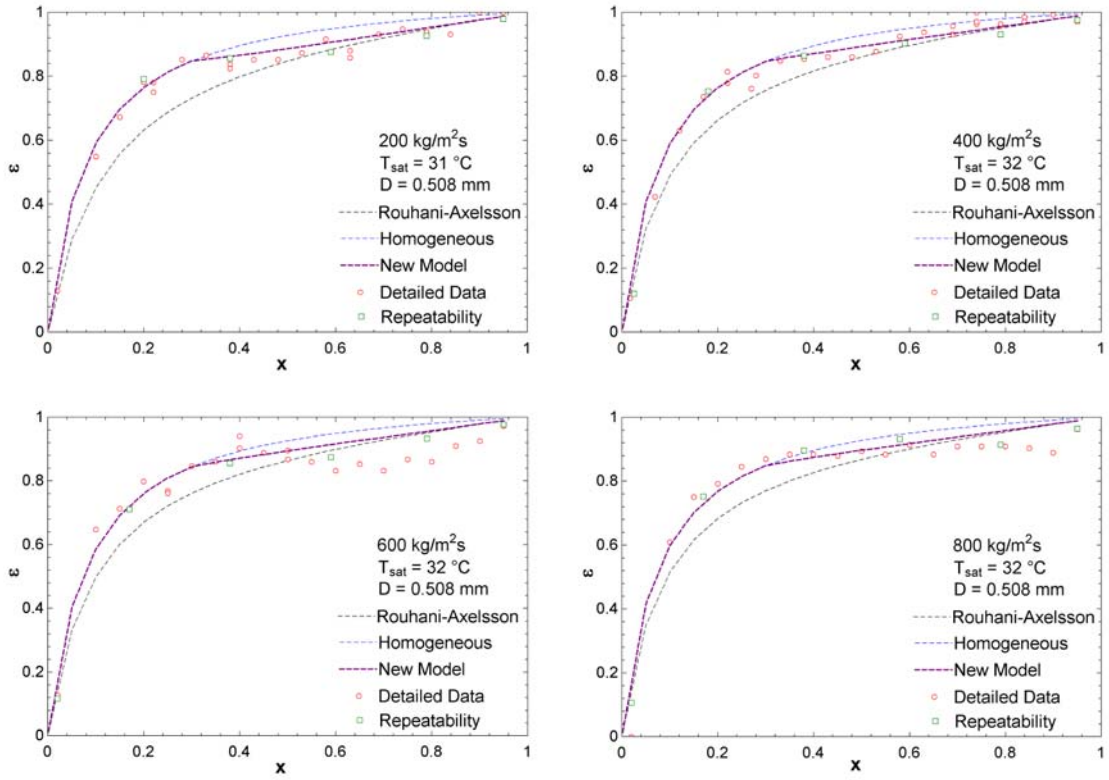

Figure 28: Void Fraction data compared with models for a 0.508 mm I.D. tube with T_{sat} approx. 32 °C.

9.0 Discussion and Modeling of Void Fraction

9.1 Existing Void Fraction Models

The most common ways of predicting void fraction are: empirical and semi-empirical methods, models based on the physics of flow regimes, models incorporating the radial distributions of the local void fraction and flow velocity, the homogeneous model, which assumes that the two phases travel at the same velocity, and one-dimensional models that account for different velocities of both phases. The homogeneous void fraction is the limiting case as the system pressure tends towards the critical pressure where the difference in phase densities disappears.

Various approaches have been attempted to predict void fraction analytically. In most instances, some quantity such as the kinetic energy of the two phases is minimized with an assumption that the flow will tend towards the minimum of this quantity. Such is the case of the widely used model presented by Zivi (1964) for annular flow, assuming that no liquid is entrained in the vapor core. The model is based on the principle that the total kinetic energy of the two phases will seek to be a minimum. This model showed good agreement with the homogeneous model at qualities greater than $x \geq 0.5$ in a calculation made by Thome (2006).

One of the leading empirical models is that of Smith (1969) who assumed a separated flow consisting of a liquid phase and a gas phase with a fraction of liquid entrained in the gas as droplets. This fraction of liquid entrainment was assigned a value empirically. He compared his model to three independent banks of void fraction data

obtained with three different techniques and was able to predict the data to within ±10%. Smith (1969) claimed that his model was valid for all conditions of two-phase flow regardless of pressure, mass flux, flow regime, and enthalpy change.

The drift flux model relates void fraction to the superficial velocity of the vapor and the superficial velocity of the liquid. Many have contributed to this model since its creation, especially Ishii (1977), who showed that this model can be used with or without reference to flow regimes. For horizontal tubes, Steiner (1993) reports that the drift flux method of Rouhani (1969) is in good agreement with experimental data. Thome (2006) presents R-410A void fraction data for an 8 mm I.D. tube at 40 °C for various mass fluxes and compared them to the Zivi (1964), the Rouhani (1969), and the homogeneous models as a reference.

The effect of mass velocity becomes more evident as it decreases. The Zivi (1964) method does not account for this effect, but the Rouhani (1969) model does. Wojtan, Ursenbacher and Thome (2004) measured 238 time-averaged cross sectional void fractions for stratified, stratified-wavy, and some slug flows for R-22 and R-410A at 5 °C inside a 13.6 mm I.D. horizontal glass tube using an optical measurement technique and they compared their data to the Rouhani (1969) model and the homogeneous model. They found that the drift flux model of Rouhani (1969) gave an average deviation of 1.5 % and a standard deviation of 14.8 % and was the best of the methods tested.

El Hajal et al. (2003) noticed that data for void fraction during adiabatic and condensing refrigerant flow in relatively large tubes tended to fall in between the Homogeneous and Rouhani-Axelsson models. To better predict the data, they recommended a logarithmic mean of the two models as $\varepsilon = \frac{\varepsilon_{hem} - \varepsilon_{RA}}{\ln\left(\frac{\varepsilon_{hem}}{\varepsilon_{RA}}\right)}$. This produces a void fraction curve that very nearly bisects the two models. As can be seen from the figures above, however, the current data do not bisect the two models but rather seem to take on truly homogeneous behavior at low vapor quality and transition to separated flow behavior at higher vapor quality.

9.2 New Void Fraction Model

It was apparent from the data that a new void fraction model was needed to predict the void fraction behavior as the tube diameter decreased. The relationship between the homogeneous equilibrium and Rouhani-Axelsson models was inescapable as well. A new model was developed based on the observation that the void fraction followed the homogeneous model until liquid slugs that bridged the tube diameter disappeared. The transition from slug to annular flow was analyzed in the classic flow regime modeling work of Taitel and Dukler (1976), who proposed that the transition from slug to annular flow occurred at a constant value of the turbulent-turbulent Lockhart-Martinelli parameter: $X_{tt} = 1.6$. Based on the void fraction data of this study, the void fraction follows the homogenous model until $X_{tt} = 1$, after which it transitions to a separated flow configuration as quality increases and X_{tt} goes to zero. (The value of $X_{tt} = 1$ is consistent with the flow regime map described in Thome (2006).) In other words, the new mini-channel void fraction, ε_{mc}, is given by

$$\varepsilon_{mc} = \xi\varepsilon_{hem} + (1-\xi)\varepsilon_{RA} \tag{17}$$

where

$$\xi = \begin{cases} 1 & if \quad X_{tt} > 1 \\ \left(1 - X_{tt}\right) & if \quad X_{tt} \le 1 \end{cases}, \tag{18}$$

$$X_{tt} = \left(\frac{1-x}{x}\right)^{0.875}\left(\frac{\rho_g}{\rho_l}\right)^{0.5}\left(\frac{\mu_l}{\mu_g}\right)^{0.125}, \tag{19}$$

$$\varepsilon_{hem} = \frac{1}{1+\left(\frac{1-x}{x}\right)\frac{\rho_g}{\rho_l}}, \tag{20}$$

and

$$\varepsilon_{RA} = \frac{x}{\rho_g}\left\{\left(1+0.12(1-x)\right)\left(\frac{x}{\rho_g}+\frac{1-x}{\rho_l}\right)+\frac{1.18(1-x)\left[g\sigma\left(\rho_l-\rho_g\right)\right]^{0.25}}{G_{tot}\rho_l^{0.5}}\right\}^{-1} \tag{21}$$

While this captured the basic trends, it did not capture the beginning of the transition between ε_{hem} and ε_{RA} correctly as a function of diameter. Thus, as was done in the pressure drop modeling, the capillary length was invoked to include the impact of surface tension on the transition to annular (or annular-like) flow. Equation (18) then becomes

$$\xi = \begin{cases} 1 & if \quad \zeta > 1 \\ \left(1 - \zeta\right) & if \quad \zeta \le 1 \end{cases} \tag{22}$$

with

$$\zeta = X_{tt}\left(\frac{\lambda}{D}\right) \tag{23}$$

where λ is the capillary length from Equation (10).

The results of this simple void fraction model can be seen in Figures 23 through 28 above, where it predicts the current data very well. Figure 29 presents a more direct comparison between the current experimental data and ε_{hem}, ε_{RA} and the new model. The new model predicts the current data to within 8.0% mean absolute error. In addition, it should extend to other tube sizes correctly, as the capillary length factor in Equation (23) eliminates the homogeneous term from the model as the diameter increases, leaving only the Rouhani-Axelsson term. On the other hand, as the tube diameter continues to decrease, the model increasingly emphasizes the homogeneous term, which is consistent with a number of studies performed in truly micro-scaled channels.

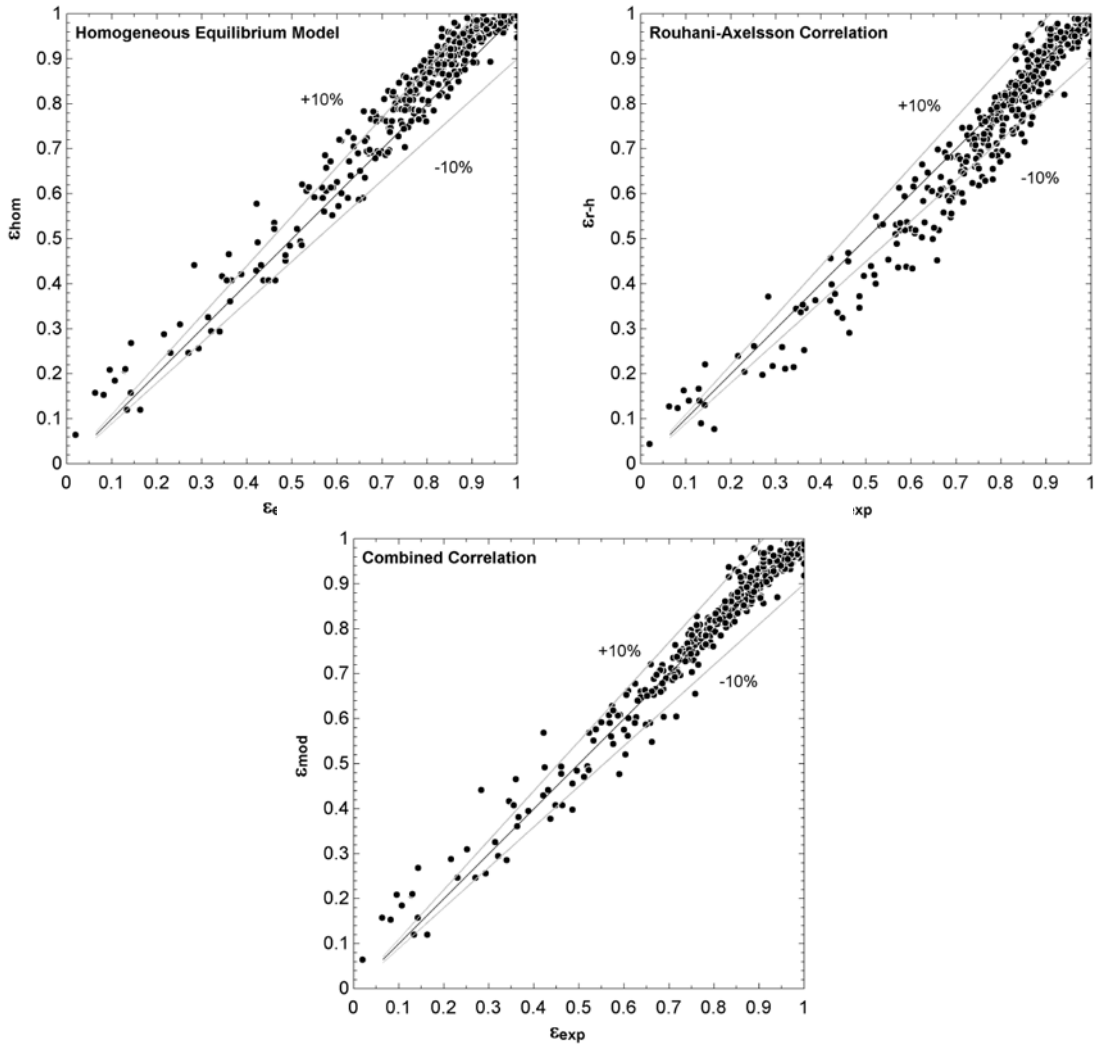

Figure 29: Comparison of void fraction models with the current data

10.0 Summary

The objective of this project was to measure the pressure drop and void fraction of R-410A at condensation conditions (i.e., $T_{sat} \sim 50$ °C) in small, single tubes of 0.5 mm, 1 mm and 3 mm in diameter. The project was to deliver models for these behaviors as well.

As is detailed in the following report, the PI and his staff achieved these objectives along with several other significant outcomes. These are summarized here:

- A ring-sensor capacitance probe was used for the first time at length scales of 3 mm and below, and a new, general method was developed for calibrating the probe in-situ, greatly increasing the accuracy and utility of the capacitive void fraction sensor
- A unique micro-channel flow facility was developed in which the flow of liquid and vapor are independently driven by separate high-pressure syringe pumps, allowing for very stable two-phase flow at a wide range of flow conditions and flow rates. In addition, this eliminated the very challenging problem of accurately measuring very small flow rates of vapor or liquid.
- As a result of the flow visualization, it was discovered that droplet entrainment is very significant in microchannel flows. The PI has not seen this behavior clearly documented in previous literature. Droplets sizes do not scale with tube diameter, so droplets with diameters that are 50% or more of the tube diameter are not uncommon in the 0.5 mm tube flows. This observation led to modeling efforts that were very successful in capturing the diameter trends in the pressure drop and void fraction.
- In order to be able to develop models with confidence, the PI and his staff extended the scope of the project to include data at $T_{sat} \sim 30$ °C. The reason for this is that the thermophysical properties of R-410A are very sensitive to temperature, and this allowed the investigators to probe the impact of these properties on the pressure drop and void fraction in addition to the impact of geometry and flow rate.
- This report presents a new interpretation of the Muller-Steinhagen and Heck correlation for pressure drop and a simple modification that allows it to accurately predict pressure drop and pressure drop trends (i.e., the peak in the pressure drop vs. quality curve) as the tube diameter decreases. While still heavily empirical, the result is general and should still retain its accuracy for large tube flows as well. This model predicted all of the current data set (no data excluded) to within 17% MAE as well as capturing all of the trends in the data correctly.
- The void fraction data indicated, in agreement with many previous researchers, that as the tube diameter decreases, the void fraction behavior

approaches that of a homogeneous mixture. However, at mid to high qualities, the void fraction reverts to "large tube" or separated flow behavior. The detailed data provided in this report are the first such data ever produced for small tubes and provide important insight into the void fraction behavior. A new model has been developed based on the data and the flow visualization that predicts the void fraction from all test sections and flows (no data excluded) to within 7% MAE. This model will extend to large tubes without modification. It is based on physical principals and appears to capture all tube geometry and fluid property variations extremely well.

Recommendations

Based on the extensive experience gained from this project, the PI recommends the following for future studies:

- Continue this work to smaller tubes and wider flow ranges using the new test facility design. This design is very flexible and can operate over a wider range of conditions than other designs reported in the literature.
- Fully characterize the entrainment behavior. It is hypothesized that droplet entrainment plays an increasingly dominant role in the two-phase flow behavior as the test section diameter decreases. Models are needed for droplet size and velocity over a wide range of operating conditions and fluid properties.
- Focus on development of a physical, phenomenological model for pressure drop in two-phase flow. It is likely that additional models for entrainment, wave generation and wave shear, among other items, will be needed.
- Explicitly incorporate entrainment into the void fraction model. With detailed droplet entrainment data, it is likely that an accurate, first-principles model can be developed for void fraction.
- It will be vitally important to add the effects of applied heat flux, both in evaporation and condensation, to this analysis. Heat flux will add significant acceleration and instability to the flow as well as impact droplet entrainment. In evaporation, the impact of a rapidly moving three-phase contact line must be quantified.

References

Ahmed, W. H., (2006). Capacitance Sensors for Void-Fraction Measurements and Flow Pattern Identification in Air-Oil Two-Phase Flow, *IEEE Sensors J.,* **6**(5) pp. 1153-1163.

Armand, A. A., Treschev, G. G., (1946). *Izv Vses Teplotek Inst* **1** 16-23.

Brito, Gurova, Mardolcar, de Castro, Nieto, (2000). Dielectric constant of the nearly azeotropic mixture R-410A,"*International Journal of Thermophysics*, **21**(2), pp 415-427.

Cavallini, A., Censi, G., Del Col, D., Doretti, L., Longo, G. A., Rossetto, L. (2000). Condensation of halogenated refrigerants inside smooth tubes. *Int J of HVAC and R Research,* **8**(4), pp. 429-451

Chen, I. Y., et al. (2002). An empirical correlation for two-phase frictional performance in small diameter tubes. *Int J of Heat and Mass Transfer* **45**, pp. 3667-3671.

Chisholm D. (1973). Pressure gradients due to friction during the flow of evaporating two-phase mixtures in smooth tubes and channels. *International Journal of Heat and Mass Transfer,* **16**, pp. 347-58.

Chung , P. M.-Y., and K. Kawaji, (2004). The effect of channel diameter on adiabatic two-phase flow characteristics in microchannels. *International Journal of Multiphase Flow*, **30**(7-8), pp. 735–761.

Churchill, S. W. (1977). Friction-factor equation spans all fluid- flow regimes. *Chemical Engineering*, **84**(24), pp. 91-92.

Elkow, K. J. and Rezkallah, K. S., (1996). Void Fraction Measurement in Gas-Liquid Using Capacitance Sensors, *Meas. Sci. Technol.*, **7**(8) pp. 1153-1163.

Friedel, L. (1980). Improved friction pressure drop correlations for horizontal and vertical two-phase pipe flow. *Int. Chem. Engr*., **20** pp. 253-67.

Fukamachi, N., T. Hazuku, T. Takamasa, T. Hibiki, and M. Ishii, (2003) Measurement on liquid film in microchannels using laser focus displacement meter. *First International Conference on Microchannels and Minichannels*, pp. 543–550.

Geraets, J. J. M., and Borst, J. C., (1988). A capacitance sensor for two-phase void fraction measurement and flow pattern identification. *Int. J. Multiphase Flow*, **14**(3), pp. 305-320.

Grönnerud R. (1979). Investigation of liquid hold-up, flow resistance and heat transfer in circulation type evaporators, part IV; two-phase flow resistance in boiling refrigerants. Annexe 1972-1, Bull. de l'Inst. du Froid.

Hewitt, G. F., (1978). *Measurement of Two-Phase Parameters*. Academic Press, London.

Hewitt, G. F., Shire, G., L., and Bott, T., R., (1994). *Process Heat Transfer*. Boca Raton: CRC Press; Begell House.

Ishii, M. (1977). One dimensional drift-flux model and constitutive equations for relative motion between phases in various two-phase flow regimes, Argonne National Laboratory, Report ANL-77-47, October, Argonne, IL.

Kattan, N., Thome, J.R., and Favrat, D. (1998a). Flow boiling in horizontal tubes. Part 1: Development of a Diabatic Two-Phase Flow Pattern Map, *J. Heat Transfer,* **120**(1), pp. 140-147.

Kawahara, A., P. M.-Y. Chung, and M. Kawaji, (2002). Investigation of two-phase flow pattern, void fraction and pressure drop in a microchannel. *International Journal of Multiphase Flow*, **28** pp. 1411–1435.

Kawahara, A., Sadatomi, M., Okayama, K., Kawaji, M. and Chung, P. M.–Y. (2005) Effects of Channel Diameter and Liquid Properties on Void Fraction in Adiabatic Two-Phase Flow Through Microchannels, *Heat Transfer Engineering*, **26**(3), pp. 13-19.

Kew, P. A., and Cornwell, K., (1997). Correlations for the prediction of boiling heat transfer in small diameter channels, *Appl. Therm. Eng.*, **17**(8-10), pp. 705-715.

Lee, H.J and Lee, S.Y. (2001). Pressure drop correlations for two-phase flow within horizontal rectangular channels with small heights. Int. J. Multiphase Flow, **27**, pp. 783-796.

Lockhart, R. W. and Martinelli, R. C. (1949). Proposed correlation of data for isothermal two-phase, two-component flow in pipes. *Chemical Engineering Progress*, **45**(1), pp. 39–48.

McDermott, B., (2008). Two phase flow regimes and their impact on pressure drop behavior. MS thesis, University of Wisconsin-Madison, Madison, Wisconsin, USA.

Mishima, K., and Hibiki, T., (1996). Some characteristics of air-water two-phase flow in small diameter vertical tubes, *Int. J. Multiphase Flow* **22**, pp. 703-712.

Müller-Steinhagen, H., and Heck, K.A. (1986). A simple friction pressure drop correlation for two-phase flow in pipes". *Chemical Engineering Processing,* **20,** pp. 297-308.

Nino, V., P. S. Hrnjak, and T. A. Newell, (2002). Analysis of void fraction in microchannels. In E. Groll, editor, *International Refrigeration Conference* at Purdue University, Purdue University.

Okada O. and H. Fujita, (1993). "Behavior of liquid films and droplets in the non-equilibrium region of downward mist flow (comparison of porous and central nozzle mixing methods). *International Journal of Multiphase Flow*, **19**(1), pp. 79-89.

Ould Didi M. B., Kattan N., and Thome J. R. (2002). Prediction of two-phase pressure gradients of refrigerants inside horizontal tubes. *International Journal of Refrigeration*, **25**, pp. 935-947.

Pawlosky, J. L., Ching, C. Y., Shoukri, M. (2004) Measurement of Void Fraction and Pressure Drop of Air-Oil Two-Phase Flow in Horizontal Pipes, *Journal of Engineering for Gas Turbines and Power,* **126** p. 107-118.

Qu, W. and Mudawar, I., (2003). Measurement and prediction of pressure drop in two-phase microchannel heat sinks, *Int. J. of Heat and Mass Transfer,* **46**, pp. 2737-2753.

Rodriguez, D. J, 2004, Characterization of bubble entrainment, interfacial roughness and the sliding bubble mechanism in horizontal annular flow. PhD thesis, University of Wisconsin- Madison, Madison, Wisconsin, USA, 2004.

Revellin, R., Thome, J. R., (2006). Adiabatic two-phase frictional pressure drops in microchannels, *Experimental Thermal and Fluid Science*, doi:10.1016/j.expthermflusci.2006.07.001

Rouhani, S. Z., (1969) AB Atomenergi, Sweden, Internal Report, AE-RTV 841.

Rouhani, S. Z., Axelsson, E., (1970). Calculation of void volume fraction in the subcooled and quality boiling regions. *Int. J. Heat Mass Transfer,* **13**, pp. 383-393.

Serizawa, A., Feng, Z., and Kawara, Z., (2002). Two-phase flow in microchannels, *Exp. Therm. Fluid Sci.,* **26**(6-7), pp. 703-714.

Shedd, Timothy A. (2013). "Two-Phase Internal Flow: Toward a Theory of Everything." *Heat Transfer Engineering.* Accepted for publication.

Smith, S. L., (1969). Void fractions in two- phase flow. A correlation based on an equal velocity head model, *Proc. Inst. Mech. Engng.,* **184**(36), pp. 647-664.

Steiner, D. (1993) *VDI-Wärmeatlas (VDI Heat Atlas),* Verein Deutscher Ingenieure, VDI-Gesellschaft Verfahrenstechnik und Chemieingeniurwesen (GCV), Dusseldorf, Chapter Hbb.

Suo M., and Griffith, P., (1964). Two-phase flow in capillary tubes *Trans. ASME: Journal of Basic Engineering,* pp. 576-582.

Thome, J.R., (2006). Engineering Data Book III. Wolvering Tube, Inc.

Tran, T. N., Chyu, M. W., Wambsganss, D. M. France, (2000). Two phase pressure drop of refrigerants during flow boiling in small channels: an experimental investigation and correlation development, *Int. J. Multiphase Flow* **26** pp. 1739-1754.

Tribe, C., and Müller-Steinhagen, H. (2000). An evaluation of the performance of phenomenological models for predicting pressure gradient during gas-liquid flow in horizontal pipelines,. *International Journal of Multiphase Flow,* **26**, pp. 1019-36.

Wadekar, V. V., (1990). Flow boiling –a simple correlation for convective heat transfer component, *Heat Transfer* **1**, pp. 87-91.

Wang, C.C., Chiang S.K., Chang, Y.J., and Chung, T.W. (2001). Two-phase flow resistance of refrigerants R-22, R-410A and R-407C in small diameter tubes. *Trans IChemE,* **79(**A)

Wojtan, L., Ursenbacher, T., Thome, J. R., (2004). Dynamic Void Fractions in Stratified Types of Flow, Part II: Measurements for R-22 and R-410a. *Int. J. Multiphase Flow,* **30**, p. 125-137.

Zhang, M., and Webb, R.L. (2001). Correlation of two-phase friction for refrigerants in small-diameter tubes. *Experimental Thermal and Fluid Science,* **25**, pp. 131-139.

Zivi, S. M., (1964). Estimation of steady-state steam void fraction by means of the principle of minimum entropy production, *Trans. Am. Soc. Mech. Engrs.,* Series C, *J. Heat Transfer* **86,** pp. 247-252.